5-2016

An Investigation Into The Effects Of Low-Dose Gamma Radiation On Porcine Digital Flexor Tendons

Megan Keira Robson
Clemson University, mrobson@g.clemson.edu

AN INVESTIGATION INTO THE EFFECTS OF LOW-DOSE GAMMA RADIATION ON PORCINE DIGITAL FLEXOR TENDONS

A Thesis
Presented to
the Graduate School of
Clemson University

In Partial Fulfillment
of the Requirements for the Degree
Master of Science
Bioengineering

---

by
Megan Keira Robson
May 2016

Accepted by:
Dr. Delphine Dean, PhD, Committee Chair
Dr. John Desjardins, PhD
Dr. Jeffrey Willey, PhD

ABSTRACT

Cancer is one of the leading causes of death worldwide and radiation therapy is used as a treatment method on millions of patients each year. While the biological response of tendon tissue to high-dose radiation has been investigated over the years, the effects of low-dose gamma radiation on tendons is not well understood. The goal of this research is to investigate the impact of clinically relevant low dose gamma radiation on tendon tissue.

Fresh tendons were harvested from mature porcine forefeet and exposed to 5 Gray of Cesium gamma radiation. Histological and chemical data were obtained over the course of five days following irradiation.

In the first phase of the study, histological aspects of the tendon were examined. Masson's Trichrome revealed an increased expression of collagen while H&E and Safranin-O found an increased occurrence of apoptosis, which was confirmed by DNA fragment end labeling.

The second phase of the study investigated the sGAG content of the tissue and culture media over time following irradiation exposure. Significant differences were seen between the control and irradiated groups in the sGAG content within the tissue (on days 3 and 5) and in the culture media (on day 5).

DEDICATION

This thesis is dedicated to my wonderful friends and family:

to my grandmother, Lala Johnson, who has provided me with endless love, wisdom, and encouragement as I follow my dreams; without her strength, guidance, and unselfish support, I would not be who I am today;

to my father, Geoffrey Robson, whose priceless advice and unique genius have been the lighthouse to guide my way;

and to my grandfather, Jimmie Johnson, for all of his support and his confidence in my ability to achieve my goals.

In Memoriam

This thesis is in memory of my mother, Donna Robson, who is not only my guardian angel, but who also serves as the foundation for my interest in medicine and my pursuit of my degrees in bioengineering.

It is also in memory of my uncle, James Clyde Robson III, who sparked my interest in bioengineering as a major and who pushed me to attend Clemson University after high school. He was able to describe the field of bioengineering to me in a way that ultimately fueled my desire to pursue a masters degree in bioengineering.

TABLE OF CONTENTS

Page

Table of Contents (Continued)

Page

LIST OF TABLES

LIST OF FIGURES

List of Figures (Continued)

List of Figures (Continued)

List of Figures (Continued)

Figure Page

CHAPTER ONE

INTRODUCTION

1.1 Motivation

Connective tissues such as tendon or cartilage were once thought to be impervious to the damaging effects of ionizing radiation. However, over the last few decades, researchers have discovered that this isn't always the case. The majority of available literature combining the study of radiation and tendons focuses on very high levels of radiation (Mrad) and its impact on massively dense tendons (e.g. rat or kangaroo tail).

Due to the increasing prevalence of cancer and the increasing use of radiotherapy to treat it, it is important to investigate the impact of clinically relevant (low-dose) ionizing radiation on tendons. This research is significant because it will allow us to see if extra precautions should be taken to protect tendons or ligaments in the immediate vicinity of a joint, bone, or muscle receiving radiation treatment.

1.2 Research Aims

In this study, we will first investigate the microscopic histological changes caused by 5 Gray (Gy) of gamma radiation. We will look for evidence of an increase in the occurrence of apoptosis in irradiated tissue, investigate levels of collagen synthesis, study the proteoglycan expression in the tissue, and examine the tissue samples for evidence of calcification following irradiation. In the next phase of this study, biochemical assays will be employed to look at apoptosis and the levels of sulfated glycosaminoglycans (sGAGs) in the tissue and culture media.

CHAPTER TWO

LITERATURE REVIEW: TENDONS

2.1 Introduction to Tendons

Tendons are part of the musculoskeletal system and serve to bridge the connection between muscles and the bones they operate. Tendons are able to transmit the forces generated by the muscles to their respective bones, allowing for joint movement. Under normal loads, tendons maintain smooth joint movement and mechanics throughout their range of motion (Lin, Cardenas, & Soslowsky, 2004). When presented with higher loads, tendons limit the range of motion to anatomical barriers (O'Brien, 1992; Lin et al., 2004). Because of this, tendons not only aid in locomotion but also help to support joints and prevent injury (Lin et al., 2004). Tendons are a type of soft connective tissue called dense fibrous connective tissue or dense regular connective tissue.

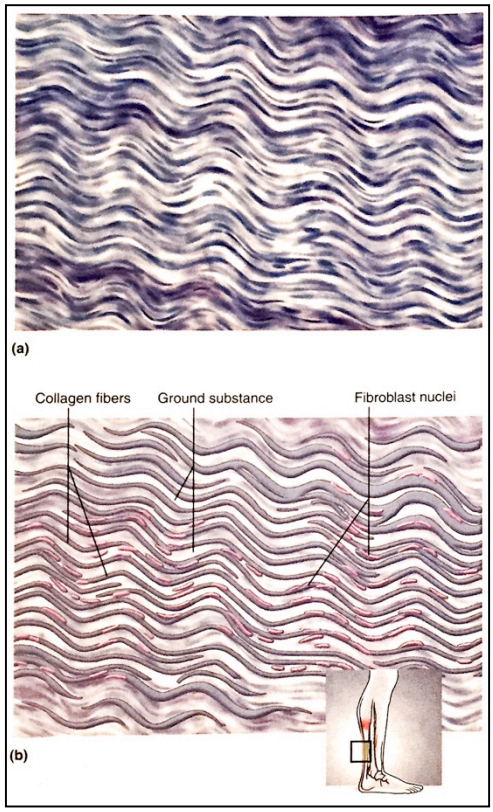

Figure 2.1: Dense regular connective tissue of a tendon (400x) (Saladin, 2012)

Dense regular connective tissue consists of closely packed collagen fibers, arranged in bundles, and oriented parallel to each other (Saladin, 2012). The parallel fiber arrangement occurs as an adaptation to the directions of stresses in musculoskeletal

tissues (Saladin, 2012). In dense regular connective tissue, the only cell types present under normal physiological conditions are specialized types of fibroblast, called tenoblasts and tenocytes (Kannus, 2000). However, under pathological conditions, other cell types infiltrate into tendon tissue, including inflammatory cells, macrophages, and/or myofibroblasts (Kannus, 2000). Tenoblasts are large, slender cells that, during tendon metabolism, are capable of producing all of the components that make up the tendon matrix (Kannus, 2000; Saladin, 2012) (Figure 2.1). The highly proliferative tenoblasts range in length between 20 and 70 μm and vary in width from 8 to 20 μm. Tenocytes, which are terminally differentiated cells, ranges from 80 to 300 μm in diameter and they have longer cellular processes (Kannus, 2000; Franchi, Trirè, Wuaranta, Orsini, & Ottani, 2007a). Tenoblast presence decreases with age as they tend to become quiescent tenocytes.

In tissue sections, there appears to be a vacant space amid the cells and fibers, as seen in Figure 2.1. This empty space is occupied by the ground substance, a featureless, gelatinous substance arising from three classes of large molecules: glycosaminoglycans (GAGs), proteoglycans (PGs), and glycoproteins (Kannus, 2000; Saladin, 2012). This substance serves to protect the fragile cells from mechanical injury by absorbing compressive forces.

2.1.1 Hierarchical Structure

The basic building block of all soft connective tissue is the collagen fibril. In order for connective tissues to form their unique functions, fibrils are arranged in a particular architecture. The hierarchical structure of connective tissue reflects and depends on different stress states under which the tissue is required to function. The commonalities within soft connective tissue starts at the molecular level with similarities in the amino acid sequences (Baer, Cassidy, & Hiltner, 1991). Unlike other classes of proteins, collagens contain hydroxyproline. Along with proline and glycine, these three amino acids make up more than fifty percent of the total amino acid content in all types of collagens. The addition of other amino acids or variations in the amino acid ratios differentiates between different collagen types. These amino acids play a significant role

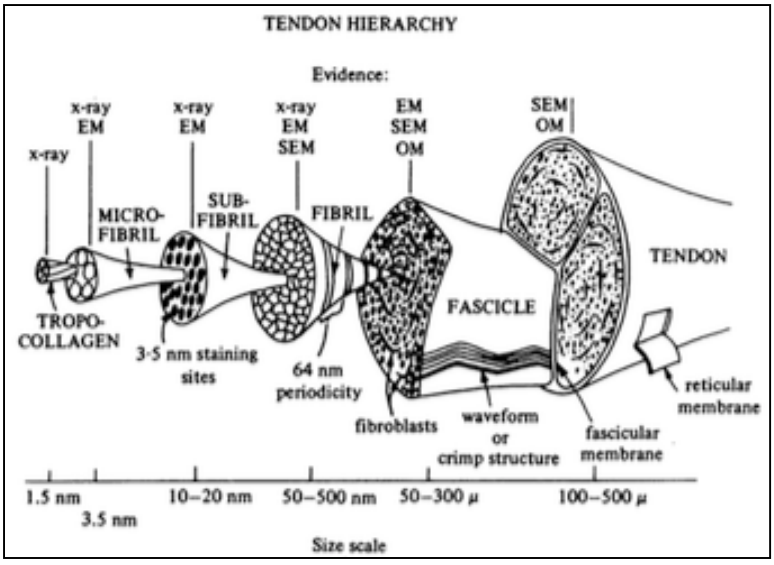

Figure 2.2: Tendon Hierarchy (Baer et al., 1991)

in determining the three dimensional conformation of collagen's precursor, the tropocollagen molecule (Baer et al., 1991).

Tropocollagen is made up of three helical polypeptide chains. Longitudinally, five tropocollagen molecules aggregate to form microfibrils, which combine to form subfibrils (Figure 2.2) (Baer et al., 1991; Wang, 2006). The quarter-staggered arrangement of tropocollagen helicies along the length of the subfibril combined with the gap between successive macromolecules creates a characteristic 64 nm banding pattern that is observed in collagen fibrils (Figure 2.3). Collagen fibrils are well stabilized as a result of the covalent intramolecular crosslinks that bind the collagen molecules together (Franchi et al., 2007b). A group of collagen fibrils then group together, forming a fascicle (or collagen fiber), which is the smallest level of the tendon hierarchy that is able to be viewed using light microscopy (Kannus, 2000). Lastly, two or three collagen fibers form a tendon (Figure 2.2). In tendons, collagen fibers are arranged in highly ordered parallel

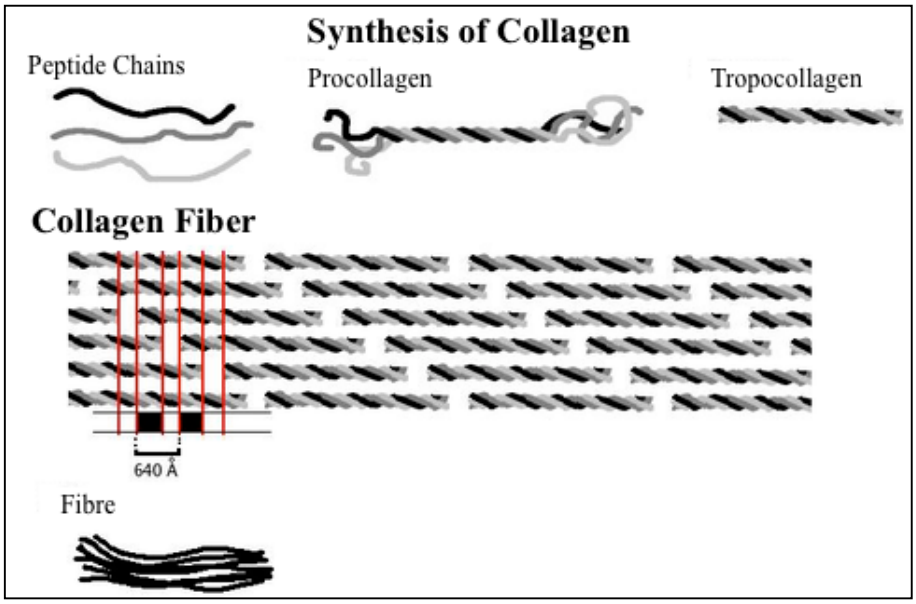

Figure 2.3: Formation of a collagen fibril from the peptide chains by successive polymerizations (Solitchka, 2005; Reproduced under CC BY-SA 3.0 license)

bundles along the length of the tendon and serve to enhance the tendon's response to mechanical loading (Franchi et al., 2007a) and resistance to tensile loads (Woo et al., 1993).

By using polarized light microscopy, a periodic waveform configuration (commonly referred to as "crimp") is visible at the fascicle level (Diamant, Keller, Baer, Litt, & Arridge, 1972; Hansen, Weiss, & Barton, 2002; Franchi et al., 2007b). The angle and length of the crimp pattern depend on the type of tendon and the location of the fibers in the tendon (Wilmink, Wilson, & Goodship, 1992).

The predominant type of collagen present in tendons is type I (Kannus, 2000; Silver, Freeman, & Seehra, 2003). Type I collagen is a co-polymer of two or more fibril-forming collagens (Silver et al., 2003; Franchi et al., 2007a). Other forms of fibrillar collagens are types II, III, V, and XI (Silver et al., 2003; Canty & Kaddler, 2005). Type I collagen is initially synthesized within cells as procollagen chains (Silver & Christiansen, 1999) and is released from cell membrane invaginations into the ECM, where the chains undergo removal of the amino (N--) and carboxyl (C--) terminal non-helical ends, becoming tropocollagen (Figure 2.4) (Silver et al., 2003; Franchi et al., 2007a, Canty &

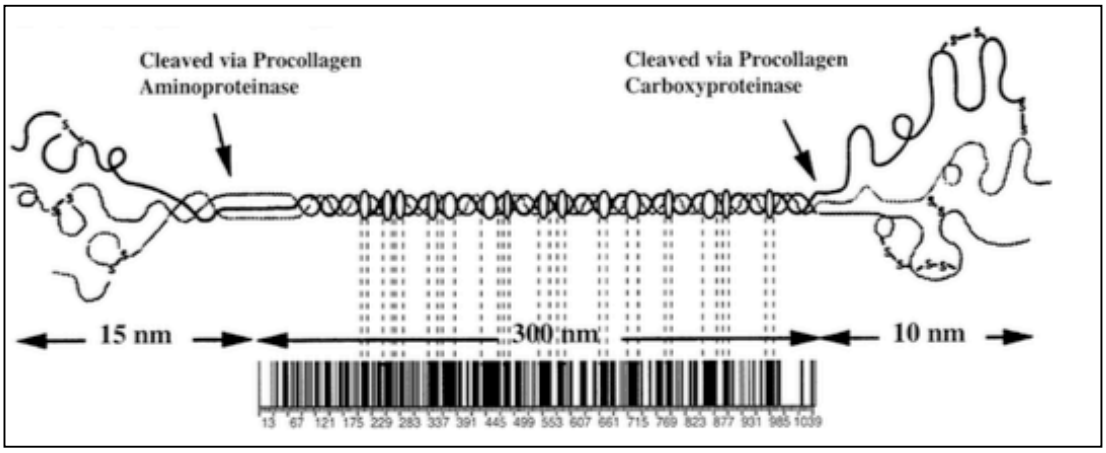

Figure 2.4: Diagram of procollagen type I molecule (Silver et al., 2003)

Kaddler, 2005). During the initial stages of tendon healing, there is an increased presence of collagen type III in the tissue in order to provide additional stabilization to the ECM (Lin et al., 2004). At the completion of the tendon healing cycle, the homeostatic balance of collagen type I to III is restored (Lin et al., 2004).

2.1.2 Tendinous Extracellular Matrix

Elastin accounts for 1-2% of a tendon's dry weight whereas collagen makes up 65-80% of dry mass (Kannus, 2000). Within a collagen fiber, the fibrils are embedded in a non-collagenous hydrophilic extracellular matrix, primarily composed of high molecular weight hyaluronic acid (HA) with a highly branched aggregate of proteoglycans (PGs) (Baer, 1991). In the extracellular matrix of the tendon there are also several glycoproteins present, including Tenascin-C and fibronectin (Wang, 2006). Tenascin-C interacts with collagen fibrils and thus contributes to the mechanical stability of the ECM (Elefteriou, Exposito, Garrone, & Lethias, 2001). Fibronectin is found on the surface of collagens and its synthesis has been reported to increase in order to facilitate wound healing (Jozsa et al., 1989, Williams, McCullagh, & Silver, 1984)

Proteoglycans (PGs) are a heterogeneous family of complex macromolecules (Silver & Christiansen, 1999). They are located intracellularly at the cell surface and in the extracellular matrix (ECM) and are composed of a core protein with one or more glycosaminoglycan (GAG) side chains (Yoon & Halper, 2005; Silver & Christiansen, 1999). The functions of PGs found in the tendon ECM are not completely understood, although research has shown that changes in their rate of turnover have been associated with tendinopathies (Riley et al., 1994). In tendons, aggrecans are constitutively

expressed and active (Rees et al., 2000). Furthermore, research indicates that aggrecan turnover in tendon is much higher than in other connective tissues such as cartilage (Waggett, Rees, & Caterson, 2004). The PGs found in tendons are primarily decorin and biglycan (Table 2.1) (Kannus, 2000; Magnusson Hansen, & Kjaer, 2003; Franchi et al., 2007a). Research has revealed that PGs and subsequently GAGs play a critical role in the biomechanics of tendon tissue. In 1997, K.G. Danielson and colleagues reported that the skin of decorin-deficient mice is unable to withstand sudden tensile strain. Furthermore, it has been revealed that the absence of decorin in the tendons of mice was shown to cause a decrease in the tendon's strength and stiffness (Zhang et al., 2006). The properties of the most abundant PGs found in tendons can be seen in Table 2.1.

Glycosaminoglycans (GAGs) are polysaccharide chains, composed of repeating disaccharide units (3-Saladin, 2012; Coulson-Thomas & Gesteria, 2014). Depending on the disaccharide unit contained in the GAG, it can be organized into one of five groups: chondroitin sulfate, dermatan sulfate, heparin sulfate, keratin sulfate, or hyaluronic acid (hyaluronan, HA) (Yoon & Halper, 2005; Coulson-Thomas & Gesteria, 2014). Hyaluronan (HA), which is found free in the ECM, is the most abundant GAG in tendon. In tendons, the concentration of GAGs is significantly less when compared to cartilage or other types of connective tissues (Yoon & Halper, 2005). Beyond their function in the tissue biomechanics, GAGs also play a pivotal role in the modulation of cell signals (Yoon & Halper, 2005).

Table 2.1: Properties and roles of the most abundant PGs found in tendons. (CS = Chondroitin Sulfate, DS = Dermatan Sulfate, KS = Keratin Sulfate) (Yoon & Halper, 2005; Iozzo & Murdoch, 1996)

Name	Size of core protein (kDa)	Type (Number) of GAG side chains	Properties and role in tendon
Decorin	36	CS/DS (1), or CS/DS (1) + KS (1)	Binds to fibrillar collagen, inhibits collagen fibrillogenesis, binds TGFb and EGF
Biglycan	38	CS/DS (1-2)	Binds to fibrillar collagen.
Fibro-modulin	42	KS (4)	Binds to type I collagen, facilitates formation of mature large collagen fibrils, modulation of tendon strength
Lumican	38	KS (2-3)	Binds to type I collagen, inhibits size of collagen fibrils, modulation of tendon strength
Aggrecan	220	CS (~100) KS (~60)	Linked to hyaluronan, provides resiliency, low levels in tensional parts of tendon, high levels in compressed regions, particularly in fibrocartilage
Versican	265-370	CS/DS (10-30)	Linked to hyaluronan, low levels in tensional parts of tendon, somewhat higher levels in compressed regions, increases viscoelasticity, maintains cell shape.

2.1.3 Tendon Coverings

Primary, secondary, and tertiary fiber bundles are each surrounded by a thin reticular connective tissue network, called the endotenon, which allows independent relative movement of the fascicles within the tendon due to its low friction coefficient (Kannus, 2000; Khan, Cook, Kannus, Maffulli, & Bonar, 2002; Rigozzi, 2011). Tertiary fiber bundles are bound together by another type of connective tissue sheath, called the epitenon, thus forming a tendon. On its inner surface, the epitenon is continuous with the endotenon (Kannus, 2000). While some tendons have true synovial sheaths, a loose areolar connective tissue sheath called the paratenon surrounds many tendons. The paratenon acts as a sleeve, allowing free movement of the tendon against surrounding

tissues, therefore reducing friction (Kannus, 2000). On its outer surface, the epitenon is continuous with the paratenon.

As previously stated, tendons connect muscles to bone. At the tendon-bone interface, there is an element called the enthesis. Entheses come in two forms: fibrous enthesis or fibrocartilaginous enthesis. The fibrous enthesis attaches to the periosteum during childhood or directly to the bone during adulthood (Wang, 2006). The fibrocartilaginous enthesis has a transitional zone of hyaline fibrocartilage, which helps to distribute the mechanical loads (Wang, 2006). The enthesis is able to bear tensile, compressive, and shear forces (Wang, 2006). Furthermore, studies have shown that tensile forces at the enthesis may be up to four times greater than at the tendon mid-substance (Wang, 2006). At the muscle-tendon, or myotendinous, junction, the tendons collagen fibrils are inserted into deep recesses formed by myoblasts (Wang, 2006). This enables the transmission of tensile forces from contractile proteins in the muscle to tendon fibers (Wang, 2006). The myotendinous junction is reported to be the weakest point of the muscle-tendon unit (Wang, 2006). Most tendons not only attach to bone, but also attach to adjacent dense fibrous connective tissue as a means of dissipating stress concentrations at the enthesis. This, in turn, reduces the risk of failure or local wear and tear (Benjamin, Kaiser, & Milz, 2008).

2.2 Biomechanics of Tendons

In response to induced mechanical loading conditions, tendons change their structure and biological behavior in response to induced mechanical loading conditions (Wang, Guo, & Li, 2012). This ability of connective tissues to alter their structure in

response to mechanical loading is called tissue mechanical adaption (or mechanoresponse) (Wang, 2006). For example, tenocytes are able to modify their behavior based on changing mechanical load (Waggett, Benjamin, & Ralphs, 2006). Additionally, research shows that, *in vitro*, tendon cells can upregulate collagen synthesis when subjected to tensional forces; this response is based on gap junctional communication (Benjamin et al., 2008). In response to appropriate levels of physical training, tenoblasts have been reported to increase production of collagen type I as well as increase their cross-sectional area and tensile strength (Tipton, Matthes, Maynard, & Carey, 1975; Suominem, Kiiskinen , & Keikinen, 1980; Michna & Hartmann, 1989; Landberg, 2001). Researchers have noted that appropriate mechanical loading has anabolic effects on tendons, strengthening them and improving their healing quality, however, excessive mechanical loading results in injury (Wang et al., 2012).

A study on the overuse of tendons showed an increase in cellularity and loss of normal collagen fiber organization, features characteristic of human tendinopathy (Soslowsky et al., 2000). The study also showed a marked decline in tendon mechanical properties, including elastic modulus and maximum stress at failure. Excessive mechanical loading conditions have been shown to cause abnormal differentiation of tendon stem cells, which could contribute to the development of tendinopathy (Zhang & Wang, 2010a; Zhang & Wang, 2010b; Wang et al., 2012). Additionally, researchers have reported that, in mice subjected to intense treadmill running, an increase in the amount of myofibroblasts was observed (Szczodry et al., 2009). Myofibroblasts are a type of activated fibroblast, involved in the repair and remodeling of injured tissues (Hinz et al., 2001, Tomasek et al., 2002). Their presence following exercise is indicative of active

repair and remodeling of the tendon tissue which might have been microinjured as a result of the imposed mechanical loading on the tendon (Wang et al., 2012).

2.2.1 Viscoelasticity and Stress-Strain Curve

The typical stress strain curve of a tendon begins with an initial toe region, in which the tendon is strained up to 2% (Figure 2.5) (Wang, 2006). This region represents the stretching out of the "crimp". As previously mentioned, the angle and length of this crimp pattern vary between and within tendons; the differences in the crimp pattern affect the tendon's mechanical properties (e.g., tendons with small crimp angle fail before those with larger crimp angle) (Wilmink et al, 1992).

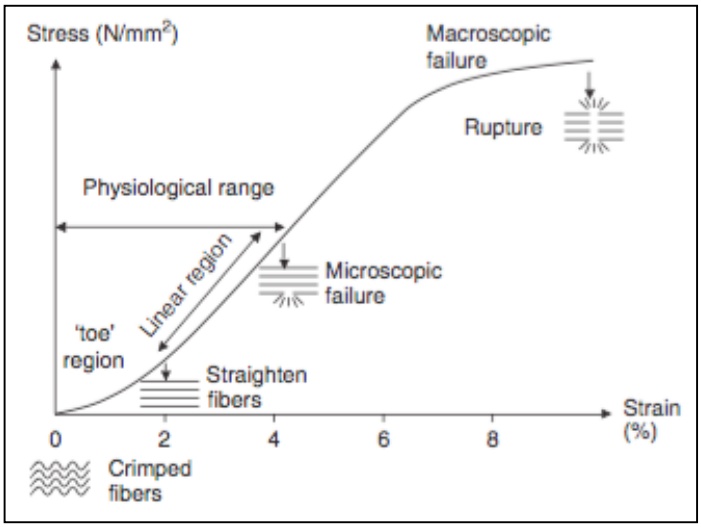

Figure 2.5: Tendon stress-strain curve (Wang, 2006)

The next section of the stress-strain curve is referred to as the linear region (Figure 2.5). In this region, the tendon is stretched less than 4% and the collagen fibers lose the crimp pattern (Wang, 2006). The slope of this region is equal to the Young's modulus of the tendon. If the tendon is stretched beyond 4%, microscopic tearing of the collagen fibers occurs (Wang, 2006). Additionally, strain beyond 8-10% will induce macroscopic failure and eventually tendon rupture (Figure 2.5) (Butler, Grood, Noyes, & Zernicke, 1987).

Similar to other soft tissues like ligaments and skin, tendons are viscoelastic and are thus sensitive to different strain rates (Wang, 2006). It is inferred that this viscoelastic behavior is due to collagen, water, and interactions collagenous proteins and non-collagenous proteins (e.g., PGs) (Wang, 2006). A tissue's viscoelasticity is defined by stress-relaxation, creep, and hysteresis (Butler et al., 1987). Due to the viscoelasticity attributed to tendons, they are more deformable at low strain rates and are therefore able to absorb more energy but are less effective at transferring loads (Wang, 2006; Wang et al., 2012). However, at high strain rates, tendons become less deformable and have a high degree of stiffness, which allows them to be more effective at moving larger muscular loads to bones (Jozsa & Kannus, 1997; Wang et al., 2012).

2.2.2 Mathematical Models

Mathematical models have been developed as a means to complement experimental studies on the mechanics of tendon behavior. They also serve to provide researchers with the potential to predict the mechanical behavior of the tissue beyond the experimental limits. Earlier models focused on describing the nonlinear aspects of a tendon's stress-strain response and ignored the time-dependent components. However, in the last 50 years, models have been developed with incorporate the time- and history-dependency of the relationship and thus the viscoelasticity (Woo et al., 1993).

2.3 Tendon Injuries and Repair

In response to tendon injury, the body initiates a series of events consisting of healing and scar formation (Lin et al, 2004). T.W. Lin and colleagues (2004) divided

these events into three separate phases: (1) hemostasis/inflammation, (2) proliferation/ fibroplasia, and (3) remodeling/maturation (Figure 2.6). The initial phase of tendon healing, hemostasis/inflammation, occurs immediately following injury. In order to stabilize the newly forming extracellular matrix, there is a significant increase in the tendon's DNA, fibronectin, GAGs, water, and collagen type III content (Lin et al., 2004; Woo et al., 2000a; Woo et al., 2000b; Joza & Kannus, 1997; Gomez, 1995; Montgomery, 1989; Grinnell, 1984). During the second phase of tendon healing, the main cell type present is fibroblasts, followed by a smaller number of macrophages and mast cells (Lin et al., 2004). An increase in the endoplasmic reticulum of fibroblasts, a clear sign of active matrix synthesis, has been shown to occur in this phase (Lin et al., 2004, Jozsa & Kannus, 1997). Collagen type III and DNA concentrations are also known to reach their peak levels during this phase (Lin et al., 2004). In the third and final stage of tendon healing, the tendon's ratio of type III to type I collagen returns to normal ranges. Furthermore, the concentrations of GAGs, water, and DNA also return to normal levels. Although, over time, the tensile strength of the injured tendon will return to a near-normal range, it will never achieve the optimal tensile strength of uninjured normal tendons (Figure 2.6) (Gomez, 1995; Lin et al., 2004).

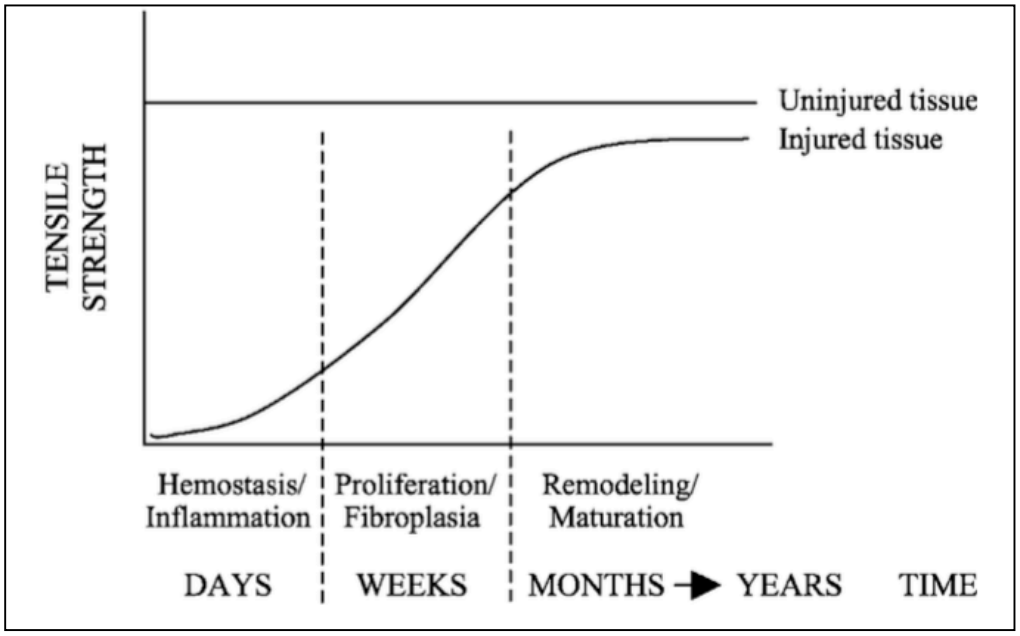

Figure 2.6: Wound-healing response in tendons divided into three phases. (Gomez, 1995; Lin et al., 2004)

2.4 References

Baer, E., Cassidy, J. J., & Hiltner, A. (1991). Hierarchical structure of collagen composite systems: Lessons from biology. *Pure and Applied Chemistry, 63*(7), 961-973.

Benjamin, M., Kaiser, E., & Milz, S. (2008). Structure-function relationships in tendons: A reveiw. *Journal of Anatomy, 212*, 211-228.

Bennett, M. B., Ker, R. F., Dimery, N. J., & Alexander, R. M. (1986). Mechanical properties of various mammalian tendons. *Journal of Zoology, London, 209*, 537-548.

Birk, D. E., & Zycband, E. (1994). Assembly of the tendon extracellular matrix during development. *Journal of Anatomy, 184*, 457-463.

Butler, D. L., Grood, E. S., Noyes, F. R., & Zernicke, R. F. (1978). Biomechanics of ligaments and tendons. *Exercise and Sport Sciences Reviews, 6*, 125–181.

Canty, E. G., & Kaddler, K. E. (2005). Procollagen trafficking, processing and fibrillogenesis. *Journal of Science, 119*, 1341-1353.

Coulson-Thomas, V. J., & Gesteria, T. F. (2014). Dimethylmethylene blue assay (DMMB). *Bio-Protocol, 4*(18), e1236. doi:bio-protocol.org/e1236

Danielson, K. G., Baribault, H., Holmes, D. F., Graham, H., Kadler K.E., & Iozzo R.V. (1997). Targeted disruption of decorin leads to abnormal collagen fibril morphology and skin fragility. *Journal of Cell Biology, 136*, 729-743.

Diamant, J., Keller, A., Baer, E., Litt, M., & Arridge, R. G. C. (1972). Ultrastructure and its relation to mechanical properties as a function of ageing. *Proceedings of the Royal Society of London, Series B, Biological Sciences, 180*(1060), 293-315.

Elefteriou, F., Exposito, J. Y., Garrone, R., & Lethias, C. (2001). Binding of Tenascin-X to decorin. *FEBS Letters, 495*, 44-47.

Franchi, M., Trirè, A., Wuaranta, M., Orsini, E., & Ottani, V. (2007a). Collagen structure of tendon relates to function. *The Scientific World Journal, 7*, 404-420.

Franchi, M., Fini, M., Quaranta, M., De Pasquale, V., Raspanti, M., Giavaresi, G., . . . Ruggeri, A. (2007b). Crimp morphology in relaxed and stretched rat achilles tendon. *Journal of Anatomy, 210*, 1-7.

Fukuta, S., Oyama, M., Kavalkovich, K., Fu, F. H., & Niyibizi, C. (1998). Identification of types II, IX and X collagens at the insertion site of the bovine achilles tendon. *Matrix Biology, 17*, 65-73.

Gomez, M. (1995). The physiology and biochemistry of soft tissue healing. In L. Griffin (Ed.), *Rehabilitation of the injured knee* (2nd ed., pp. 34–44). St. Louis, MO: Mosby Company.

Grinnell, F. (1984). Fibronectin and wound healing. *Journal of Cellular Biochemistry, 26*, 107-116.

Hansen, K. A., Weiss, J. A., & Barton, J. K. (2002). Recruitment of tendon crimp with applied tensile strain. *Journal of Biomechanical Engineering, 124*(1), 72-77.

Hinz, B., Giuseppe, C., Tomasek, J., Gabbiani, G., & Chaponnier, C. (2001). Myofibroblasts and mechano-regulation of connective tissue remodelling. *Molecular Biology of the Cell, 12*, 2730-2741.

Iozzo, R. V., & Murdoch, A. D. (1996). Proteoglycans of the extracellular environment: Clues from the gene and protein side offer novel perspectives in molecular diversity of function. *FASEB Journal, 10*(5), 598-614.

Jozsa, L., Lehto, M., Kannus, P., Kvist, M., Reffy, A., Vieno, T., . . . Elek, E. (1989). Fibronectin and laminin in achilles tendon. *Acta Physiologica Scandinavica, 60*, 469–471.

Jozsa, L., & Kannus, P. (1997). *Human tendons: Anatomy, physiology, and pathology.* Champaign, IL: Human Kinetics.

Jung, H.-J., Fisher, M. B., & Woo, S. L.-Y. (2009). Role of biomechanics in the understanding of normal, injured, and healing ligaments and tendons. *Sports Medicine, Arthroscopy, Rehabilitation, Therapy & Technology, 1*(9).

Kahn, K. M., Cook, J. L., Kannus, P., Maffulli, N., & Bonar, S. F. (2002). Time to abandon the tendinitis myth. *BMJ, 324*, 626-627.

Kannus, P. (2000). Structure of the tendon connective tissue. *Scandinavian Journal of Medicine & Science in Sports, 10*, 312-320.

Langberg, H., Rosendal, L., & Kjaer, M. (2001). Training-induced changes in peritendinous type I collagen turnover determined by microdialysis in humans. *Journal of Physiology, 534*, 297–302.

Lin, T. W., Cardenas, L., & Soslowsky, L. J. (2004). Biomechanics of tendon injury and repair. *Journal of Biomechanics, 37*, 865-877.

Magnusson, S. P., Hansen, P., & Kjaer, M. (2003). Tendon properties in relation to muscular activity and physical training. *Scandinavian Journal of Medicine & Science in Sports, 13*, 211-233.

Magnusson, S. P., Qvortrup, K., Larsen, J. O., Rosager, S., Hanson, P., Aagaard, P., . . . Kjaer, M. (2002). Collagen fibril size and crimp morphology in ruptured and intact achilles tendons. *Matrix Biology, 21*, 369-377.

Michna, H., & Hartmann, G. (1989). Adaptation of tendon collagen to exercise. *International Orthopaedics, 13*, 161-165.

Montgomery, R. D. (1989). Healing of muscle, ligaments, and tendons. *Seminars in Veterinary Medicine and Surgery (Small Animal), 4*, 304-311.

O'Brien, M. (1992). Functional anatomy and physiology of tendons. *Clinical Journal of Sport Medicine, 11*(3), 505-520.

Ogele, T. (2013). Fibrous conenctive tissue. Retrieved from http://cnx.org/contents/bea6f848-5d6e-4695-a9b7-38a51dde8c0b@1/Fibrous-Connective-Tissue

Raspanti, M., Congiu, T., & Guizzardi, S. (2002). Structural aspects of the extracellular matrix of the tendon: An atomic force and scanning electron microscopy study. *Archives of Histology and Cutology, 65*(1), 37-43.

Rees, S. G., Flannery, C. R., Little, C. B., Hughes, C. E., Caterson, B., & Dent, C. M. (2000). Catabolism of aggrecan, decorin and biglycan in tendon. *Biochemical Journal, 350*(I), 181-188.

Rigozzi, S. (2011). *Structure and function in tendon: Experimental studies on the ultrastructural determinants of tendon biomechanical function* (Doctor of Sciences). (Diss. ETH No. 19668).

Riley, G. P., Harrall, R. L., Constant, C. R., Chard, M. D., Cawston, T. E., & Hazleman, B. L. (1994). Glycosaminoglycans of human rotator cuff tendons: Changes with age and in chronic rotator cuff tendinitis. *Annals of Rheumatic Diseases, 53*(6), 367-376.

Saladin, K. S. (2012). *Anatomy & physiology, the unity of form and function* (6th ed.). New York, NY: McGraw-Hill Companies, Inc.

Silver, F. H., & Christiansen, D. L. (1999). Biomaterials science and biocompatibility. New York: Springer-Verlang.

Silver, F. H., Freeman, J. W., & Seehra, G. P. (2003). Collagen self-assembly and the development of tendon mechanical properties. *Journal of Biomechanics, 36*, 1529-2553.

Solitchka (2005). *Formation d'une fibre de collagène à partir des chaînes peptidiques, par polymérisations successives.* Reproduced under Creative Commons ShareAlike 3.0 License.

Soslowsky, L. J., Thomopoulos, S., Tun, S., Flanagan, C. L., Keefer, C. C., Mastaw, J., & Carpenter, J. E. (2000). Overuse activity injures the supraspinatus tendon in an

animal model: A histologic and biomechanical study. *Journal of Shoulder and Elbow Surgery, 9*, 79-84.

Suominen, H., Kiiskinen, A., & Heikkinen, E. (1980). Effects of physical training on metabolism of connective tissues in young mice.*Acta Physiologica Scandinavica, 108*, 17-22.

Szczodry, M., Zhang, J., Lim, C., Davitt, H. L., Yeager, T., Fu, F. H., & Wang, J. H. -. (2009). Treadmill running exercise results in the presence of numerous myofibroblasts in mouse patellar tendons. Journal *of Orthopaedic Research,* 1373-1378.

Tipton, C. M., Matthes, R. D., Maynard, J. A., & Carey, R. A. (1975). The influence of physical activity on ligaments and tendons. *Medicine and Science in Sports, 7*, 165-175.

Tomasek, J., Gabbiani, G., Hinz, B., Chaponnier, C., & Brown, R. (2002). Myofibroblasts and mechanoregulation of connective tissue remodeling. *Nature Review Molecular Cell Biology, 3*, 349-363.

Waggett, A. D., Rees, S. G., & Caterson, B. (2004). Increased turnover of proteoglycan aggregates in tendon *vs*. cartilage. *International Journal of Experimental Pathology, 85*(4), A76-A77.

Waggett, A. D., Benjamin, M., & Ralphs, J. R. (2006). Connexin 32 and 43 gap junctions differentially modulate tenocyte response to cyclic mechanical load. *European Journal of Cell Biology, 85*, 1145-1154.

Wang, J. H.-C. (2006). Mechanobiology of tendon. *Journal of Biomechanics, 39*, 1563-1582.

Wang, J. H.-C., Guo, Q., & Li, B. (2012). Tendon biomechanics and Mechanobiology—A minireview of basic concepts and recent advancements. *Journal of Hand Therapy, 25*, 133-141.

Williams, I. F., McCullagh, K. G., & Silver, I. A. (1984). The distribution of types I and III collagen and fibronectin in the healing equine tendon. *Connective Tissue Research, 12*, 211-227.

Wilmink, J., Wilson, A. M., & Goodship, A. E. (1992). Functional significance of the morphology and micromechanics of collagen fibres in relation to partial rupture of the superficial digital flexor tendon in racehorses. *Research in Veterinary Science, 53*, 354–359.

Woo, S. L.–Y., Johnson, G. A., & Smith, B. A. (1993). Mathematical modeling of ligaments and tendons. *Journal of Biomechanical Engineering, 115*, 468-473.

Woo, S. L.-Y., An, K., Frank, C., Livesay, G., Ma, A., Zeminski, J., . . . Myers, B. (2000a). Anatomy, biology, and biomechanics of tendon and ligament. In J. Buckwalter, T. Einhorn & S. Simon (Eds.), *Orthopaedic basic science: Biology and biomechanics of the musculoskeletal system* (2nd ed., pp. 582-616). Rosemont, IL: American Academy of Orthopaedic Surgeons.

Woo, S. L.-Y., Debski, R. E., Zeminski, J., Abramowitch, S. D., Saw, S. S., & Fenwick, J. A. (2000b). Injury and repair of ligaments and tendons. *Annual Review of Biomedical Engineering, 2*, 83-118.

Woo, S. L.-Y., Abramowitch, S. D., Kilger, R., & Liang, R. (2006). Biomechanics of knee ligaments: Injury, healing, and repair. *Journal of Biomechanics, 39*, 1-20.

Yoon, J. H., & Halper, J. (2005). Tendon proteoglycans: Biochemistry and function. *Journal of Musculoskeletal Neuronal Interactions, 5*(1), 22-34.

Zhang, G., Ezura, Y., Chervoneva, I., Robinson, P. S., Beason, D. P., Carine, E. T., . . . Birk, D. E. (2006). Decorin regulates assembly of collagen fibrils and acquisition of biomechanical properties during tendon development. *Journal of Cellular Biochemistry, 98*, 1436-1449.

Zhang, J., & Wang, J. H.-C. (2010a). Mechanobiological response of tendon stem cells: Implications of tendon homeostasis and pathogenesis of tendinopathy. *Journal of Orthopaedic Research*, 639-643.

Zhang, J., & Wang, J. H.-C. (2010b). Production of PGE(2) increases in tendons subjected to repetitive mechanical loading and induces differentiation of tendon stem cells into non-tenocytes. *Journal of Orthopaedic Research, 28*(2), 198-203.

CHAPTER THREE

LITERATURE REVIEW: RADIATION

3.1 Introduction to Radiation

3.1.1 Types of Radiation

Radiation is defined as the emission and propagation of energy from a source through space or matter in the form of waves or energized particles (Donya, Radford, ElGuindy, Firmin, & Yacoub, 2014). There are two main types of radiation, ionizing and nonionizing (Figure 3.1). When people think of radiation, they generally think of ionizing radiation, such as x-rays or gamma (γ) rays. However, there are many common types of nonionizing radiation, including thermal radiation, radio waves, microwaves, infrared light, visible light, and most ultraviolet (UV) light. When compared to ionizing

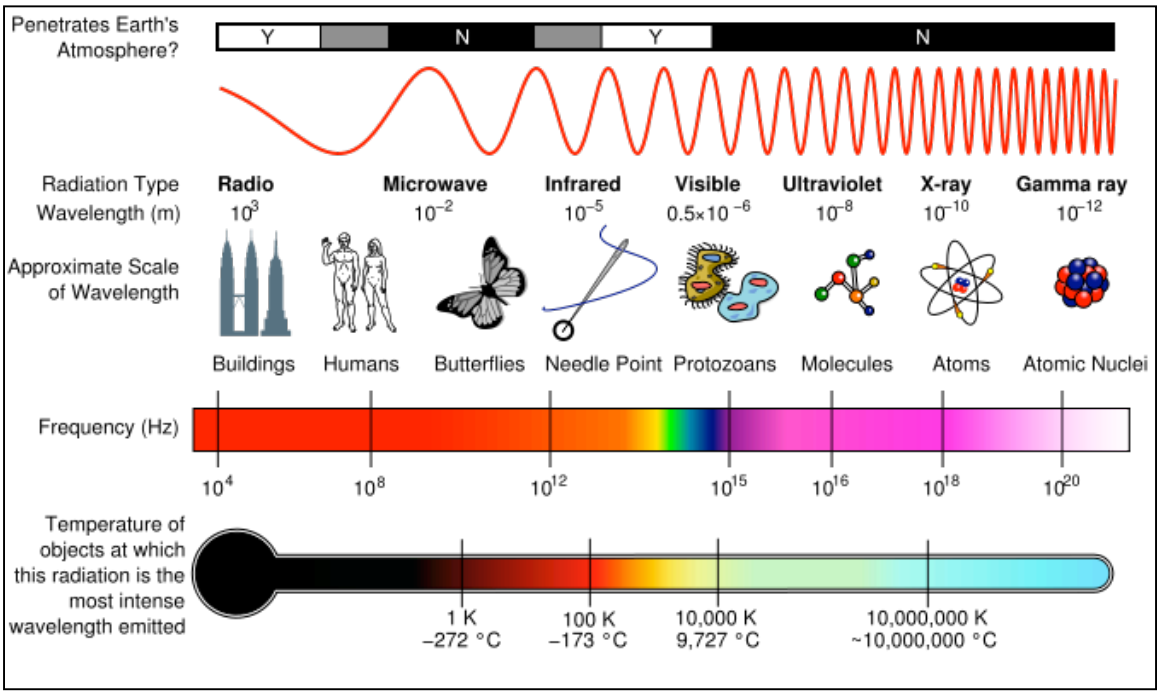

Figure 3.1: Electromagnetic Radiation Spectrum with Radiation Types (U.C. Davis Chem. Wiki, Figure reproduced under the CC BY-NC-SA 3.0 license)

radiation, nonionizing radiation has longer wavelengths, lower frequencies, and insufficient energy per quantum to ionize matter (Environmental Protection Agency, 2015). Although nonionizing radiation is generally considered safer than ionizing radiation, some forms have been shown to cause damage similar to that of ionizing radiation. For example, while small amounts of UV radiation are essential to the production of vitamin D, prolonged human exposure to solar UV radiation may result in photoaging, immunosuppression, and ultimately photocarcinogenesis (Matsumura & Ananthaswamy, 2004). At the molecular level, UV radiation causes damage to DNA. Furthermore, the UV radiation present in sunlight has been classified as an environmental human carcinogen (Matsumura & Ananthaswamy, 2004).

Ionization is defined as the transfer of enough energy to a medium that is sufficient to overcome the binding energy of an electron, causing the electron to be ejected from the atom, thus forming an ion (Mettler & Upton, 1995). Ionizing radiation deposits a relatively large amount of energy into a small area when compared to other types of radiation (Mettler & Upton, 1995). There are four main types of ionizing radiation: alpha particles, beta particles, x-rays, and gamma (γ) rays. Alpha particles are emitted from the decay of only the heaviest radioactive nuclei, such as uranium or radium (Donya et al., 2014). While very

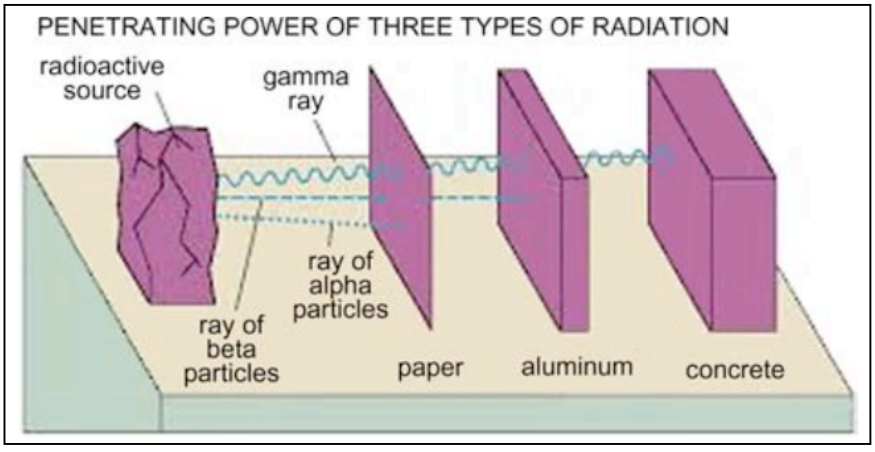

Figure 3.2 Graphic showing penetrating power of alpha, beta, & gamma radiation (Donya et al., 2014; Christiansen 1988)

energetic and highly ionizing, the weight and size of alpha particles cause them to lose energy over a small distance, allowing them to easily be stopped by paper or skin (Donya et al., 2014) (Figure 3.2). Only when inhaled or ingested are alpha particles dangerous due to highly focused ionization, which causes severe damage at both cellular and genetic levels (Rutherford, 1911; Krane, 1988). Compared to alpha particles, beta particles are much smaller and only carry about half of the electrical charge of alpha particles (Mettler & Upton, 1995). Beta particles have a much greater penetration range, and are capable of traveling several feet through the air and a few millimeters into tissue, but are easily stopped by clothing or a thin sheet of aluminum (Donya et al., 2014). However, because their ionization is spaced over a larger area, beta particles cause less damage than alpha particles. Unlike alpha and beta particles, X-rays and γ-rays do not have mass or charge. γ-rays have a significantly higher penetration range, requiring several inches of lead or several feet of concrete to stop them, while X-rays are generally less penetrating due to their lower energy (Donya et al., 2014). X-rays are known to occur naturally, but, as discovered by Roentgen, can also be produced by machines and are used every day throughout the world in the form of medical imaging machines (x-ray, CT scan, MRI, etc.) and airport security scanners, to name a few. Because γ-rays can easily pass through the whole human body, they have the potential to cause severe damage to tissue and DNA. This unique capability of γ-rays has been harnessed for use in medical science, in the form of radiation therapy for cancer (Donya et al., 2014; Hamada & Fujmichi, 2014).

The main types of ionizing radiation can be further categorized into two categories: electromagnetic radiation or particulate radiation. X-rays and γ-rays fall under the category of electromagnetic radiation while electrons, protons, neutrons, alpha

particles, and beta particles are types of particulate radiation (Azzam, Jay-Gerin, & Pain, 2012). Alpha and beta particle radiation are further categorized as directly ionizing, meaning that the charged particles (α and β particles) strike the tissue or medium and interact directly with the target molecules. X-rays and γ-rays are categorized as indirectly ionizing, meaning that they give up their energy in various interactions. The energy is then used to produce a fast moving charged particle, like an electron, which then secondarily interacts with the target molecule (Mettler & Upton, 1995).

X-rays and γ-rays have many of the same properties. As previously stated, they are massless and carry no charge. They also both originate from energy released by unstable atoms; γ-rays originate from the nucleus and x-rays originate from the electrons. Unlike alpha and beta particle radiation, x-rays and γ-rays have a long penetration range and are made up of photons, which are massless particles that represent quanta or packets of energy transmitted in the form of wave motion (Martin & Harbison, 1996). The amount of energy contained in each quantum is inversely proportional to the wavelength of the radiation (Martin & Harbison, 1996). In other words, the shorter the wavelength, the higher the energy. The wavelengths of electromagnetic radiation vary over a wide range, as seen in Table 3.1.

Table 3.1: Wavelengths of electromagnetic radiation (Martin & Harbison, 1996)

Type of Radiation	Wavelength, λ (metres)
Radio waves, long wave	1500
Radio waves, VHF	3
Visible light	10^{-6} to 10^{-7}
X-rays, 50 keV energy	2.5×10^{-11}
γ-rays, 1 MeV energy	1.2×10^{-12}

3.1.2 Radiation Units of Measurement

There are four units for measuring radiation: radioactivity, exposure, absorbed dose, and effective dose (Donya et al., 2014). Radioactivity is the measurement of the spontaneous nuclear transformation or radioactive decay of radionuclides (Turner, 2007). In order to measure the radioactivity of a substance, the number of nuclei that decay per unit time is measured (Close & Ludwig, 2000). The standard international (SI) unit for radioactivity is the becquerel (Bq). One bequerel is equal to one disintegration per second (Table 3.2) Close & Ludwig, 2000; Bertulani, 2007). The radioactivity of a unit weight of a substance is the specific activity, measured in becquerel per gram (Bq/g) (Close & Ludwig, 2000). The specific activity allows the comparison of different radioactivity levels between substances (Close & Ludwig, 2000). Exposure is a measure of the amount of ionizations produced by electromagnetic radiation in the air (Turner, 2007). The traditional unit of measurement for exposure is the roentgen (R), which is equal to 2.58x10-4 coulomb per kilogram (of air). Coulomb per kilogram ($\frac{C}{kg}$) is the SI unit of measurement for exposure (Table 3.2).

Table 3.2: Measurements of radiation and their respective units. (Close & Ludwig, 2000; Turner, 2007; Bertulani, 2007)

Measurement	Traditional Unit	SI Unit
Radioactivity	Curie (Ci); $1\ \text{Ci} = 3.7\times10^{10}\text{dps}$	Becquerel (Bq); $1\ \text{Bq} = 1\ \text{dps} = 0.27\times10^{-10}\text{Ci}$
Exposure	Roentgen (R); $1\ \text{R} = 2.58\times10^{-4}\ \frac{\text{C}}{\text{kg of air}}$	Coulomb/kilogram (C/kg) of air
Absorbed Dose	Radiation absorbed dose (rad); $1\ \text{rad} = 100\ \frac{\text{erg}}{\text{g}}$	Gray (Gy); $100\ \text{rad} = 1\ \text{Gy} = 1\ \frac{\text{J}}{\text{kg}}$
Equivalent Dose	Roentgen equivalent man (rem); 1 rad = 1 rem	Sievert (Sv); 1 Sv = 100 rem
Linear Energy Transfer (LET)	$\frac{\text{keV}}{\mu\text{m}} = 10\frac{\text{MeV}}{\text{cm}}$	Newton (N); $1\ \text{MeV} = 1.602\times10^{-13}\text{Nm}$

To evaluate the hazard resulting from biological exposure to radiation, the absorbed dose must be computed. Absorbed dose is a point function that measures the energy imparted to a defined mass of tissue (Eichholz & Poston, 1967; Bertulani, 2007; Close & Ludwig, 2000; Turner, 2007). The traditional unit for measuring absorbed dose is the rad (radiation absorbed dose): 1 rad = 10^{-2} J/kg of material (Table 3.2). However, the SI unit for absorbed dose is the Gray (Gy): 1 Gy = 1 J/kg = 100 rad (Table 3.2).

Another measurement of dose, equivalent dose (also referred to as radioactive dose equivalent), was introduced to allow for different levels of biological effectiveness of different kinds of radiation (Turner, 2007). Equivalent dose is a point function and measures the absorbed dose and the biological effects of the specific type of radiation observed (Turner, 2007). The formula to calculate the equivalent dose is $H = D \times W_R$, where H is the dose equivalent, D is the absorbed dose, and W_R represents the weighting

factor, as seen in Table 3.3. The traditional unit of measurement for equivalent dose is the roentgen equivalent man (rem), whereas the SI unit is the sievert (Sv) (Table 3.2). The weighting factor represents the relative biological effectiveness (RBE) of the radiation and serves to provide an absorbed dose that is representative of the various types of radiation and the energies associated with them. The relationship between these measurements and their respective SI units can be seen in Figure 3.3.

In the early 1950s, the concept of linear energy transfer (LET) was introduced in order to characterize the rate of energy transfer per unit distance along a charged-particle track (Turner, 2007). LET is therefore synonymous with stopping power. LET is usually expressed in units of keV/μm of water, which converts to 10 MeV/cm (Table 3.2) (Turner, 2007). According to the National Institute of Standards and Technology (NIST), there currently is not an SI unit for LET (NIST, 2015).

Table 3.3: Weighting factors for different types of radiation according to the International Council on Radiological Protection Report 103 (International Commission on Radiological Protection, 2007)

Radiation Type	Energy	W_R
α particles		20
β particles		1
X-rays, gamma rays		1
Neutrons	< 1 MeV	$2.5 + 18.2e^{-\frac{[\ln(E)]^2}{6}}$
	1 - 50 MeV	$5.0 + 17.0e^{-\frac{[\ln 2E]^2}{6}}$
	> 50 MeV	$2.5 + 3.25e^{-\frac{[\ln(0.04E)]^2}{6}}$
Protons		2
Heavy nuclei		20

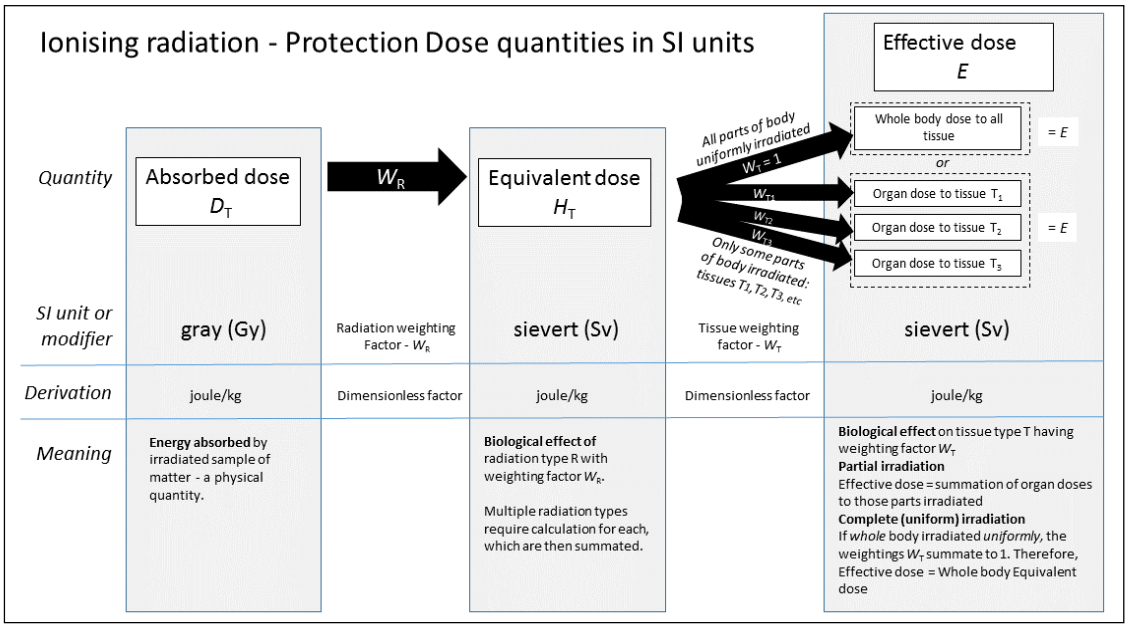

Figure 3.3: Graphic displaying the relationship between different measurements of radiation dose. (Doug Sim, figure reproduced under CC BY--SA 3.0 license)

3.2 Biological Effects of Radiation

The biological effects of radiation depend on the amount of energy transferred to the tissue (Mettler & Upton, 1995). At low doses, radiation is known to initiate an only partially understood chain of events, leading to cancer or genetic damage and, additionally, cell death (U.N. Environment Programme, 1991). Although the effects of low-dose radiation are not clearly understood, they are of increasing societal importance in varied aspects such as routine cancer screenings, frequent air travel, occupational exposure (especially in the field of nuclear power), manned space travel, or the potential for radiological terrorism (Table 3.3) (Brenner et al., 2003).

Table 3.4: Approximate mean doses relevant to societal low-dose radiation exposures and to low-dose radiation risk estimation (Brenner et al., 2003)

	Approximate mean individual dose, mSv*
Some societally relevant exposures	
Round-trip flight, New York to London	0.1
Single screening mammogram (breast dose)	3
Background dose due to natural radiation exposure	3/yr
Dose (over a 70-year period) to 0.5 million individuals in rural Ukraine in the vicinity of the Chernobyl accident	14
Dose range over 20-block radius from hypothetical nuclear terrorism incident [FASEB scenario 1: medical gauge containing cesium (6)]	3–30
Pediatric CT scan (stomach dose from abdominal scan)	25
Radiation worker exposure limit (1)	20/yr
Exposure on international space station	170/yr
Some low-dose epidemiological studies	
A-bomb survivors [mean dose in LSS cohort (2)]	200
Medical x-rays [breast dose in scoliosis study (4)]	100
Nuclear workers [mean dose from major studies (5)]	20
Individuals diagnostically exposed in utero (3)	10
* NOTE: Sivert measures equivalent dose and Grey measures absorbed dose. 1 mSv = 1 mGy (see Figure 3.3).	

3.2.1 Oxidative Changes

Research has shown that oxidative changes continue to occur days or even months after the initial radiation exposure. This is thought to be a result of continuous generation of reactive oxygen (ROS) and reactive nitrogen (RNS) species (Petkau, 1987; Azzam et al., 2012). At normal levels, ROS/RNS take part in signal transduction functions that are essential to healthy survival (Azzam et al., 2012; Finkel, 2000). However, at aberrant levels, they function as toxic agents and have been associated with abnormal cell proliferation (Azzam et al., 2012; Oberley & Oberley, 1988). Furthermore, these processes are not only limited to the irradiated cells but are also seen in their progeny as well as in bystander cells by means of intercellular communication mechanisms (Azzam,

Toledo, & Little, 2003; Mothersill & Seymour, 2004; Kryston, Georgiev, Pissis, & Georgakilas, 2011; Azzam et al., 2012). This knowledge is of utmost importance because the perseverance of these stressful events in progeny cells has numerous implications for long-term health risks, including but not limited to the emergence of a second malignancy following radiotherapy treatments (Azzam et al., 2012; Hall, 2004; Cucinotta & Chappell, 2010; National Research Council of the National Academies, 2005). Furthermore, there is increasing evidence supporting the role of chronic oxidative stress in the progression of degenerative diseases and radiation-induced late tissue injury (Azzam et al., 2012; Spitz, Azzam, Li, & Gius, 2004; Schonfeld et al., 2010; Zhao & Robbins, 2009).

Cells respond to the increased generation of reactive species and up-regulate signaling cascades to in response to the increased stress conditions, for example research has shown that following exposure to low LET radiations (X- & gamma- rays), adaptive responses encompassing DNA repair and antioxidation reactions may be triggered (de Toledo et al., 2006; Feinendegen, Pollycove, & Neumann, 2007; Wolff, 1998). Additionally, metabolic protections are mobilized during and soon after the insult at molecular, cellular, tissue, and organism levels (Azzam et al., 2012; Feinendegen, Brooks, & Morgan, 2011). DNA repair mechanisms are upregulated, antioxidants scavenge excess ROS, proteases remove oxidized proteins, some cellular immune responses are activated, and cells/tissues may downregulate oxidative metabolism in order to lower the concentrations of reactive chemical species (Azzam et al.,, 2012; Buonanno, de Toledo, Pain, & Azzam, 2011; Pandey, de Toledo, Pain, & Azzam, 2006; Ina & Sakai, 2005). The track structure (LET) of the impacting radiation is critical to

determine the nature of long-term effects on oxidative metabolism (Buonanno et al., 2011; Buonanno, de Toledo, & Azzam, 2011). Depending on the radiation dose, dose-rate, and radiation quality, the protective mechanisms elicited by the cells may not be adequate to cope with the induced stresses. It has been reported that approximately 60 ROS per nanogram of tissue are generated within less than a microsecond following a hit from ^{137}Cs gamma rays and that a nuclear concentration of ROS of that magnitude can cause extensive oxidative injury and modify normal biochemical reactions (Nikjoo, Goodhead, Charlton, & Paretzke, 1991; Sutherland, Bennett, Sidorkina, & Laval, 2000).

Furthermore, in irradiated cells, disturbances in the oxidative metabolism and chronic inflammatory responses may cause an increase in the levels of ROS and RNS, leading to long-term effects on genomic stability (Azzam et al., 2012).

3.2.2 Radiation-Induced Genomic Instability

Genomic instability is characterized by a high frequency of mutations in the mammalian genome (Morgan, Day, Kaplan, McGhee, & Limoli, 1996). Ionizing radiation can interfere with various metabolic pathways, specifically those which govern DNA duplication or serve to maintain the integrity of the information encoded by DNA. This interference causes genomic instability, which leads to an increase in the frequency of mutations, gene amplification, and karyotypic alterations (Morgan et al., 1996). Furthermore, cellular exposure to ionizing radiation results in a variety of directly- and indirectly-induced DNA lesions, including DNA base alterations, DNA-DNA and DNA-protein crosslinks, and single- and double-strand breaks (Ward, 1988; Morgan et al., 1996).

Irradiation induces many biological responses in a cell, such as the initiation of signal transduction pathways, activation of gene transcription, repair of damaged DNA, and cell cycle-specific growth arrest (Morgan et al., 1996; Weichselbaum, Hallahan, Sukhatme, Dritschilo, Sherman, & Kufe, 1991; Ward, 1984). Early events are likely to be factors in the irradiated cell's later fate; in other words, whether the cell will necrose, senesce, apoptose, or ultimately survive and proliferate (Morgan et al., 1996). If the cell survives, the initial biological response to the radiation may have bearing on whether the cell carries on as normal, acquires a limited lifespan, or subsequently proliferates and, by means of genomic instability, begins to take on the characteristics of a normal cell transitioning into a cancerous cell (Morgan et al., 1996).

In addition to immediate biological responses, several delayed effects in the progeny of irradiatied cells have been identified. These delayed effects include giant cell formation, cell fusion, delayed mutation, and delayed chromosomal instability (Morgan et al., 1996; Seymour, Mothersill, & Alper, 1986; Chang & Little, 1992; Mothersill & Seymour, 1987).

3.2.2 Radiation-Induced Cell Death

Ionizing radiation causes single & double strand breaks in DNA, an event that is generally lethal (Grasl-Kraupp, Ruttkay-Nedecky, Koudelka, Bukowska, Bursch, & Schulte-Hermann, 1995; Cohen-Jonathan, Bernhard, & McKenna, 1999). Irradiation also damages the cell membrane, thus inducing pathways that may cause or contribute to cell death (Cohen-Jonathan et al., 1999). There are two ways by which radiation can lead to cell death: via apoptosis or necrosis. Apoptosis is defined as programmed cell death and

is considered to be an active process of cellular suicide (Cohen-Jonathan et al., 1999). Apoptotic cells are characterized by loss of membrane integrity following DNA degradation (Wyllie, Kerr, & Currie, 1980; Dewey, Ling, & Meyn, 1995). On the other hand, necrosis is considered to be a passive process resulting from cells containing unrepaired DNA breaks and lethal chromosomal aberrations from passing through mitosis (Cohen-Jonathan et al., 1999). In necrotic cells, the integrity of the membrane is lost prior to DNA degradation (Wyllie et al., 1980; Dewey et al., 1995). DNA degradation in necrotic cells is generally random without proof of specificity in size ranges, while in apoptotic cells, DNA degradation seems to be restricted to certain size ranges (Olive, Frazer, & Banath, 1993, Dewey et al., 1995). It is hypothesized that apoptosis is programmed by specific signals in the cell that causes an endonuclease to cleave DNA at internucleosomal sites (Dewey et al., 1995). Morphologically, apoptosis is initiated by condensation of nuclear chromatin, then blebbing of the nuclear and cytoplasmic membranes, and lastly by formation of membrane-bound apoptotic bodies (Wyllie, 1992; Grasl-Kraupp et al., 1995; Cohen-Jonathan et al., 1999). The onset of apoptosis varies between cell types. It can occur immediately after irradiation (interphase death, fast apoptosis), after G2 arrest, or after one or more cell divisions (late apoptosis) (Radford, Murphy, Radley, & Ellis, 1994; Dewey et al., 1995; Yanagihara et al., 1995; Cohen-Jonathan et al., 1999).

3.3 Radiation Therapy for Cancer

Radiation therapy is used in the field of oncology to manage or treat various forms of cancer. It uses high-energy radiation to shrink tumors and kill cancer cells

(Lawrence, Ten Haken, & Giaccia, 2008). The radiation kills the cancer cells by damaging their DNA either directly or indirectly via the creation of free radicals (National Cancer Institute, 2010). Once the cell's DNA is damaged beyond repair, the cells stop dividing and die. They are then broken down and removed by the body's natural processes. While radiation therapy targets cancer cells, normal cells can also be damaged or killed, resulting in negative side effects.

Radiation therapy can be given both with curative or palliative intent. Curative intent means that the treatment is administered with the hope that it will cure a cancer by eliminating a tumor, preventing recurrence of the cancer, or both (Lawrence et al., 2008). On the other hand, palliative intent means that the therapy is not intended to cure the cancer but instead to relieve symptoms and/or reduce a patient's suffering (National Cancer Institute, 2010).

There are three ways in which radiation therapy can be given to patients: external-beam radiation therapy, internal radiation therapy (or brachytherapy), or systemic radiation therapy (National Cancer Institute, 2010). External-beam radiation therapy comes from a radiation source outside of the body while brachytherapy comes from a radioactive material that is placed inside the body near the cancer cells. Systemic radiation therapy involves a radioactive substance, given orally or intravenously, which travels to the tissues by way of the bloodstream. The choice of radiation therapy prescribed by the oncologist depends on various factors, including the type, size, or location of the cancer.

External beam radiation therapy is usually delivered in the form of photon beams (x-rays or γ-rays) (Lawrence et al., 2008). This form of treatment is usually administered

in fractionated doses; in other words, given in daily treatment sessions over the course of several weeks. The main reason for daily treatment fractions is two-fold: first, to minimize the damage to normal tissues, and secondly to increase the likelihood that the cancer cells are exposed to radiation at critical points in their cell cycle when they are most susceptible to DNA damage (Lawrence et al., 2008, Connell & Hellman, 2009).

In internal radiation therapy, or brachytherapy, radioactive isotopes are sealed in tiny pellets and placed in patients via a carrier such as needles or catheters. As these isotopes naturally decay, they give off radiation that damages neighboring cancer cells. Examples of where these pellets could be placed include interstitial brachytherapy, where the source is placed within the tumor tissue, or intracavitary brachytherapy, where the source is placed within a surgical or body cavity. This form of treatment may be able to deliver higher doses of radiation to some forms of cancer than external beam therapy while causing less damage to normal tissues (Patel & Arthur, 2006; Lawrence et al., 2008).

Brachytherapy can be used alone or in addition to external-beam radiation therapy (Patel et al., 2006). During systemic radiation therapy, the patient either swallows or is injected with a radioactive substance, like radioactive iodine or a radioactive substance bound to a monoclonal antibody (National Cancer Institute, 2010). Radioactive iodine (^{131}I) is commonly used to treat some types of thyroid cancer because thyroid cells naturally take up ^{131}I. For some other forms of cancer, the monoclonal antibody helps take the radioactive substance to the correct location.

Radiation therapy is known to cause both acute and chronic side effects. While acute side effects occur during treatment, the chronic side effects occur months or years

after the end of treatment (Lawrence et al., 2008). Factors that contribute to the side effects include the area of the body being treated, the dose given per day, the total dose given, the patient's medical condition, or any other treatments being given at the same time (National Cancer Institute, 2010).

3.4 References

Azzam, E. I., Jay-Gerin, J.-P., & Pain, D. (2012). Ionizing radiation-induced metabolic oxidative stress and prolonged cell injury. *Cancer Letters, 327*, 48–60.

Azzam, E. I., Toledo, S. M., & Little, J. B. (2003). Oxidative metabolism, gap junctions and the ionizing radiation-induced bystander effect. *Oncogene, 22*, 7050-7057.

Bailey, A. J., Rhodes, D. N., & Cater, C. W. (1964). Irradiation-induced crosslinking of collagen. *Radiation Research, 22*(4), 606-621.

Bailey, A. J. (1968). Effect of ionizing radiation on connective tissue components. In D. A. Hall (Ed.), *International review of connective tissue research* (4th ed., pp. 233-280). New York, New York: Academic Press.

Bailey, A. J., & Tromans, W. J. (1964). Effects of ionizing radiation on the ultrastructure of collagen fibrils. *Radiation Research, 23*(1), 145-155.

Bertulani, C. A. (2007). *Nuclear physics in a nutshell* (1st ed.). NJ: Princeton University Press.

Brenner, D. J., Dollc, R., Goodhead, D. T., Hall, E. J., Land, C. E., Little, J. B., . . . Zaidern, M. (2003). Cancer risks attributable to low doses of ionizing radiation: Assessing what we really know. *Proceedings of the National Academy of Sciences, 100*(24), 13761–13766.

Buonanno, M., de Toledo, S. M., Pain, D., & Azzam, E. I. (2011). Long-term consequences of radiation-induced bystander effects depend on radiation quality and dose and correlate with oxidative stress. *Radiation Research, 175*(4), 405-415.

Buonanno, M., de Toledo, S. M., & Azzam, E. I. (2011). Increased frequency of spontaneous neoplastic transformation in progeny of bystander cells from cultures exposed to densely-ionizing radiation. *PloS One, 6*(6), e21540.

Chang, W. P., & Little, J. B. (1992). Delayed reproductive death as a dominant phenotype in cell clones surviving X-irradiation. *Carcinogenesis, 13*(6), 923-928.

Christiansen, D. M., Iddins, C. J., & Sugarman, S. L. (2014). Ionizing radiation injuries and illnesses. *Emergency Medicine Clinics of North America*, 32(1), 245-265.

Close, D., & Ledwidge, L. (2000). Measuring radiation: Terminology and units/Devices and methods. *Science for Democratic Action, 8*(4), 8-14.

Cohen-Jonathan, E., Bernhard, E. J., & McKenna, W. G. (1999). How does radiation kill cells? *Current Opinion in Chemical Biology, 3*, 77-83.

Connell, P. P., & Hellman, S. (2009). Advances in radiotherapy and implications for the next century: A historical perspective. *Cancer Research*, 62(2), 383-392.

Cucinotta, F. A., & Chappell, L. J. (2010). Non-targeted effects and the dose response for heavy ion tumor induction. *Mutation Research, 687*, 49-53.

Dewey, W. C., Ling, C. C., & Meyn, R. E. (1995). Radiation-induced apoptosis: Relevance to radiotherapy. *International Journal of Radiation Oncology, 33*(4), 781-796.

Donya, M., Radford, M., ElGuindy, A., Firmin, D., & Yacoub, M. H. (2014). Radiation in medicine: Origins, risks and aspirations. *Global Cardiology Science and Practice,* 57.

Doug Sim, *Ionising Radiation, Protective Dose Quantities in SI Units*. Reproduced under Creative Commons ShareAlike 3.0 License.

Eichholz, G. G., & Poston, J. W. (1967). *Principles of nuclear radiation detection* (1st ed.). MI: Ann Arbor Science Publishers, Inc.

Environmental Protection Agency. (2015). Radiation protection. Retrieved from http://www.epa.gov/radiation

Fajardo, L. F. (2005). The pathology of ionizing radiation as defined by morphologic patterns. *Acta Oncologica, 44*, 13-22.

Feinendegen, L. E., Pollycove, M., & Neumann, R. D. (2007). Whole-body responses to low-level radiation exposure: New concepts in mammalian radiobiology. *Experimental Hematology, 35*, 37-46.

Feinendegen, L. E., Brooks, A. L., & Morgan, W. F. (2011). Biological consequences and health risks of low-level exposure to ionizing radiation: Commentary on the workshop. *Health Physics, 100*(3), 247-259.

Finkel, T. (2000). Redox-dependent signal transduction. *FEBS Letters, 476*, 52-54.

Grasl-Kraupp, B., Ruttkay-Nedecky, B., Koudelka, H., Bukowska, K., Bursch, W., & Schulte-Hermann, R. (1992). In situ detection of fragmented DNA (TUNEL assay) fails to discriminate among apoptosis, necrosis, and autolytic cell death: A cautionary note. *Hepatology, 21*(5), 1465-8.

Hall, E. J. (2004). The crooked shall be made straight; dose–response relationships for carcinogenesis. *International Journal of Radiation Oncology, 80*(5), 327-337.

Hamada, N., & Fujmichi, Y. (2014). Classification of radiation effects for dose limitation purposes: History, current situation, and future prospects. *Journal of Radiation Research*, 55(4), 629-640.

Ina, Y., & Sakai, K. (2005). Activation of immunological network by chronic low-dose-rate irradiation in wild-type mouse strains: Analysis of immune cell populations and surface molecules. *International Journal of Radiation Biology, 81*(10), 721-729.

International Commission on Radiological Protection. 2007. The 2007 recommendations of the international commission on radiological protection. Annals of the ICRP 37: 1-141.

Krane, K. S. (1988). Alpha decay. *Introductory nuclear physics* (2nd ed., pp. 246-269) John Wiley & Sons.

Kryston, T. B., Georgiev, A. B., Pissis, P., & Georgakilas, A. G. (2011). Role of oxidative stress and DNA damage in human carcinogenesis. *Mutation Research, 711*, 193–201.

Lawrence, T. S., Ten Haken, R. K., & Giaccia, A. (2008). Principles of radiation oncology. In V. T. DeVita, T. S. Lawrence & S. A. Rosenberg (Eds.), *Cancer: Principles and practice of oncology* (8th ed.). Philadelphia: Lippincott Williams and Wilkins.

Lindberg, C. A. (2012). *The effects of low dose ionizing radiation exposure on the metabolic and mechanical properties of articular cartilage.* (M.S.). Clemson University.

Martin, A., & Harbison, S. A. (1996). *An introduction to radiation protection* (4th ed.) Chapman & Hall Medical.

Matsumura, Y., & Ananthaswamy, H. N. (2004). Toxic effects of ultraviolet radiation on the skin. *Toxicology and Applied Pharmacology, 195*, 298 – 308.

Mettler, F. A., & Upton, A. C. (1995). *Medical effects of ionizing radiation* (2nd ed.). Philadelphia, PA: W.B. Saunders Company.

Morgan, W. F., Day, J. P., Kaplan, M. I., McGhee, E. M., & Limoli, C. E. (1996). Genomic instability induced by ionizing radiation. *Radiation Research, 146*(3), 247-258.

Mothersill, C., & Seymour, C. B. (1987). The influence of lethal mutations on the quantification of radiation transformation frequencies. *International Journal of Radiation Biology and Related Studies in Physics, Chemistry and Medicine, 51*, 723-729.

Mothersill, C., & Seymour, C. B. (2004). Radiation-induced bystander effects — implications for cancer. *Nature Reviews | Cancer, 4*, 158-164.

National Cancer Institute. (2010). Radiation therapy for cancer. Retrieved from http://www.cancer.gov/about-cancer/treatment/types/radiation-therapy/radiation-fact-sheet

National Institute of Standards and Technology. (2015). The NIST reference on Constants, Units, and uncertainty. Retrieved from http://physics.nist.gov

National Research Council of the National Academies, Health risks from exposure to low levels of ionizing radiation: Board on Radiation Effects Research, Division on Earth and Life Studies, Environmental Protection Agency, BEIR-VII, Phase 2 (2005).

Negrini, S., Gorgoulis, V. G., & Halazonetis, T. D. (2010). Genomic instability — an evolving hallmark of cancer. *Nature Reviews-Molecular Cell Biology, 11*, 220-228.

Nikjoo, H., Goodhead, D. T., Charlton, D. E., & Paretzke, H. G. (1991). Energy deposition in small cylindrical targets by monoenergetic electrons. *International Journal of Radiation Biology, 60*, 739-756.

Oberley, L. W., & Oberley, T. D. (1988). Role of antioxidant enzymes in cell immortalization and transformation. *Molecular and Cellular Biochemistry, 84*, 147-153.

Olive, P. L., Frazer, G., & Banath, J. P. (1993). Radiation-induced apoptosis measured in TK6 human B lymphoblast cells using the comet assay. *Radiation Research, 136*, 130-136.

Pandey, B. N., Gordon, D. M., de Toledo, S. M., Pain, D., & Azzam, E. I. (2006). Normal human fibroblasts exposed to high- or low-dose ionizing radiation: Differential effects on mitochondrial protein import and membrane potential. *Antioxidants & Redox Signaling, 8*, 153-1261.

Patel, R. R., & Arthur, D. W. (2006). The emergence of advanced brachytherapy techniques for common malignancies. *Hematology/Oncology Clinics of North America*, 20(1), 97-118.

Petkau, A. (1987). Role of superoxide dismutase in modification of radiation injury. *British Journal of Cancer, 55*, 87-95.

Radford, I. R., Murphy, T. K., Radley, J. M., & Ellis, S. L. (1994). Radiation response of mouse lymphoid and myeloid cell lines. part II. apoptotic death is shown by all lines examined. *International Journal of Radiation Biology, 65*, 217-227.

Rasmussen, T. J., Feder, S. M., Butler, D. L., & Noyes, F. R. (1994). The effects of 4 mrad of γ irradiation on the initial mechanical properties of bone-patellar tendon-bone grafts. *The Journal of Arthroscopic and Related Surgery, 10*(2), 188-197.

Rodemann, H. P., & Blaese, M. A. (2007). Responses of normal cells to ionizing radiation. *Seminars Radiation Oncology, 17*, 81-88.

Roe, S. C., Milthorpe, B. K., True, K., Rogers, G. J., & Schindhelm, K. (1992). The effect of gamma irradiation on a xenograft tendon bioprosthesis. *Clinical Materials, 9*, 149-154.

Rutherford, E. (1911). The scattering of α and β Particles by matter and the structure of the atom. *Philosophical Magazine*, 6(21).

Schonfeld, S. J., Bhatti, P., Brown, E. E., Linet, M. S., Simon, S. L., Weinstock, R. M., . . . Sigurdson, A. J. (2010). Polymorphisms in oxidative stress and inflammation pathway genes, low-dose ionizing radiation, and the risk of breast cancer among US radiologie technologists. *Cancer Causes and Control, 21*(11), 1857-1866.

Seymour, C. B., Mothersill, C., & Alper, T. (1986). High yields of lethal mutations in somatic mammalian cells that survive ionizing radiation. *International Journal of Radiation Biology, 50*, 167-179.

Spitz, D. R., Azzam, E. I., Li, J. J., & Gius, D. (2004). Metabolic oxidation/reduction reactions and cellular responses to ionizing radiation: A unifying concept in stress response biology. *Cancer and Metastasis Reviews, 23*(311-322)

Stone, H. B., Coleman, C. N., Anscher, M. S., & McBride, W. H. (2003). Effects of radiation on normal tissue: Consequences and mechanisms. *The Lancet Oncology, 4*, 529–536.

Sutherland, M., Bennett, P. V., Sidorkina, O., & Laval, J. (2000). Clustered DNA damages induced in isolated DNA and in human cells by low doses of ionizing radiation. *Proceedings of the National Academy of Sciences of the United States of America, 97*, 103-108.

de Toledo, S. M., Asaad, N., Venkatachalam, P., Li, L., Howell, R. W., Spitz, D. R., & Azzam, E. I. (2006). Adaptive responses to low-dose/low-dose-rate γ-rays in normal human fibroblasts: The role of growth architecture and oxidative metabolism. *Radiation Research, 166*, 849-857.

Tubiana, M. (2009). Can we reduce the incidence of second primary malignancies occurring after radiotherapy? A critical review. *Radiotherapy and Oncology, 91*, 4-15.

Turner, J. E. (2007). *Atoms, radiation, and radiation protection.* Weinheim, Germany: WILEY-VCH Verlag GmbH & Co.

U.N. Environment Programme (1991). *Radiation: Doses, effects, risks* (2nd ed.). Cambridge, Mass.: Blackwell Publishers.

University of Califonia at Davis ChemWiki. *Electromagnetic Spectrum with Radiation Types.* Reproduced under Creative Commons Noncommercial-ShareAlike 3.0 license.

Ward, J. F. (1984). Biochemistry of DNA lesions. *Radiation Research, 104*(2), S103-S111.

Ward, J. F. (1988). DNA damage produced by ionizing radiation in mammalian cells: Identities, mechanisms of formation, and reparability. *Progress in nucleic acid research and molecular biology* (pp. 95-125).

Weichselbaum, R. R., Hallahan, D. E., Sukhatme, V., Dritschilo, A., Sherman, M. L., & Kufe, D. W. (1991). Biological consequences of gene regulation after ionizing radiation exposure. *Journal of the National Cancer Institute, 83*, 480-484.

Wolff, S. (1998). The adaptive response in radiobiology: Evolving insights and implications. *Environmental Health Perspective, 106*(Suppl. 1), 277-283.

Wyllie, A. H., Kerr, J. F. R., & Currie, A. R. (1980). Cell death: The significance of apoptosis. *International Review of Cytology, 68*, 251-306.

Wyllie, A. H. (1992). Apoptosis and the regulation of cell numbers in normal and neoplastic tissues: An overview. *Cancer and Metastasis Reviews, 11*, 95-103.

Yanagihara, K., Nii, M., Numoto, M., Kamiya, K., Tauchi, H., Sawada, S., & Seito, T. (1995). Radiation-induced apoptotic cell death in human gastric epithelial tumor cells; correlation between mitotic death and apoptosis. *International Journal of Radiation Biology, 67*, 677-685.

Zhao, W., & Robbins, M. E. (2009). Inflammation and chronic oxidative stress in radiation-induced late normal tissue injury: Therapeutic implications. *Current Medicinal Chemistry, 16*, 130-143.

CHAPTER 4

MATERIALS AND METHODS

4.1 Tissue Harvest and Culture

Digital flexor tendons were excised from the forefeet of hogs (Vaughns' Meat Processing Co., Greer, SC). In a sterile dissection hood, the tendons were carefully removed, cut to a length of approximately 20 ± 0.20 mm (Figure 4.1), and placed in an anti-microbial wash containing protease inhibitors, 2 mM phenyl sulfonyl fluoride, 5 mM EDTA, 5 mM N-ethylmaleimide, and 5 mM benzamidine hydrochloride for 20 minutes (Appendix A). For each foot, four samples were taken, two for the control group and two for the irradiated group. After 20 minutes, the tendon sections were rinsed with media (Appendix B), divided into groups, and placed in sample cups containing 20 mL of the same media. The tendon sections remained in the media for a minimum of 24 hours prior to irradiation. During this time, the samples were cultured at 37°C and 5% CO_2 in low-glucose Dulbecco's Modified Eagle's Medium (DMEM) (Gibco) supplemented with 10% fetal bovine serum (FBS) (Atlanta Biologicals, Lawrenceville, GA), and 1% nonessential amino acids. The tendon media was then changed 4 hours prior to irradiation and again every 48 hours after irradiation. The media of the non-irradiated samples was changed at the same times as that of the irradiated samples.

Figure 4.2: Porcine tendon in dissection hood, measuring before cutting

4.2 Gamma Irradiation

After the tendon samples were equilibrated for at least 24 hours in tissue culture conditions, the media was replaced with fresh media approximately four hours prior to irradiation (30 minutes to 1 hour before leaving Clemson and taking the samples to Wake Forest Baptist Health Center in Winston-Salem, North Carolina). All harvested tendon samples were transported in a mobile incubation unit (United Laboratory Plastics, Fenton, MO) for irradiation via gamma rays from a Cesium-source radiation unit at Wake Forest Baptist Health. The samples to be irradiated received a dose of 5 Gray (Gy) Cesium gamma rays. Even though they were not irradiated, the control samples were transported to Wake Forest Baptist Health alongside the irradiated samples in order to control for any issues that might occur during the travel between institutions.

4.3 Histology

On days 3 and 5 post-irradiation, samples were taken from both the control and irradiated groups and placed in 10% Neutral Buffered Formalin (NBF) for 24 – 48 hours. The sections were then cut to a thickness of

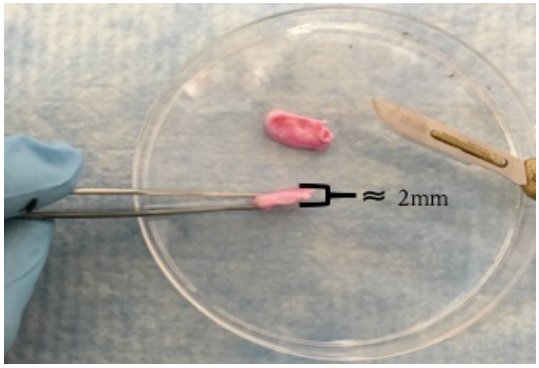

Figure 4.2: Tissue sections cut to approx. 2mm thickness in petri dish in serile conditions

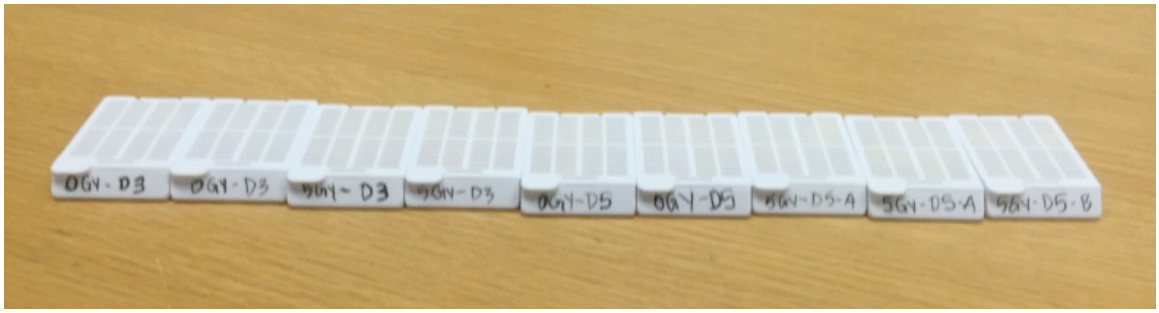

Figure 4.3: Tendon tissue samples in cassettes before going into tissue processor

approximately 2 mm in preparation for tissue processing (Figure 4.2). The samples were placed in tissue processing cassettes based on category and placed in a tissue processor for 8 hours. Following processing, the samples were placed in a warming tray and embedded in paraffin (TissueTek®, Sakura, Torrance, CA).

4.3.1 H&E, Masson's Trichrome, Safranin-O, and Alizarin Red-S

Using a microtome (Lecia Biosystems, Buffalo Grove, IL), the samples were mounted on charged slides and placed in an oven (VWR Scientific Inc., Radnor, PA) at 60°C for a minimum of 48 hours prior to histological staining. The tissue sections mounted on charged slides were stained with Hemotoxalin & Eosin (Appendix D), Masson's Trichrome (Appendix E), Safranin-O (Appendix F), and Alizarin Red S (Appendix G). Detailed protocols are in the appendices.

Hemotoxylin is a basic, positively charged stain which binds to basophilic substances like DNA and RNA and stain them purple. Eosin is an acidic, negatively charged stain that binds to acidophilic substances, namely positively charged amino acid side chains, staining them pink. Together, they make up the H&E stain. H&E stains collagen pale pink, muscle deep pink, acidophilic cytoplasm red, basophilic cytoplasm purple, nuclei blue, and erythrocytes bright red. This stain allows for observation of the samples to look for morphological signs of apoptosis prior to application of a chemical assay to highlight DNA fragmentation. A clear morphological change associated with apoptosis is a specific pattern of chromatin condensation, made visible by the hematoxylin, which is of crucial importance for diagnostic purposes (i.e. oncological diagnosis) (Fischer, Jacobson, Rose, & Zeller, 2008).

Masson's Trichrome is a stain which uses three different dyes to selectively stain muscle, collagen fibers, fibrin, and erythrocytes. Clinically, it is used to differentiate between collagen and smooth muscle in tumors and to show an increase in collagen presence in tissue, usually as a result of certain diseases. A red, acidic dye, Biebrich scarlet, binds to the acidophilic tissue components. The sample is then treated with phospho acids, which pull the red dye out of the collagen while the less permeable tissue components retain the Biebrich scarlet (University of Utah, 2016). The application of aniline blue then colors the collagenous tissue components blue (University of Utah, 2016). After completion of the Masson's Trichrome staining protocol, the muscle/keratin is stained red, cytoplasm appears pink, cell nuclei are dark brown to black, and collagen is a vivid blue (Appendix E).

The Safranin-O staining method is generally used for the detection of cartilage, mucin, and mast cell granules in formalin-fixed, paraffin-embedded tissue sections (Appendix F). Safranin-O is a cationic stain that stains acidic proteoglycans (PGs) present in tissue sections (Takara Bio Inc.). Safranin-O is used to detect aggrecan and collagen (Takara Bio Inc.) in orthopedic tissues. As previously mentioned, there is a significant presence of aggrecan in tendon tissue. Therefore, if radiation results in an increase or decrease in levels of PGs in the tendon matrix, this can be identified by examining the samples for an increased presence of Safranin-O in the irradiated samples. The counterstain, fast green, is a sulfate-group-containing substrate which strongly stains the non-collagen sites by binding strongly to the amino group of proteins. When this stain is applied to tissue sections, the nuclei stain black; the cytoplasm stains a grey-green color; and mucin, and mast cell granules stain orange to red.

Alizarin Red S is a staining procedure that is used to detect microcrystalline phosphate salts. Clinically, it is used to detect calcium deposits in liver tissue. In tissue sections, calcium forms Alizarin Red S—Ca complexes in a chelation process. The end product is birefringent. The Alizarin Red S allows identification of calcium deposits by dying them an orange to red color.

4.4 *In Situ* Apoptosis Detection

Apoptosis detection was carried out using the TACS ® 2 TdT-DAB *In Situ* Apoptosis Detection Kit (Trevigen Inc., Gaithersburg, MD) (Appendix H). This kit was designed for the detection of cellular apoptosis in tissue sections. The data obtained from this assay is to be used in conjunction with morphological data obtained via standard microscopy.

Terminal deoxynucleotidyl Transferase (TdT) binds to the exposed 3'-OH ends of DNA fragments generated in response to apoptotic signals and catalyzes the addition of biotin-labeled deoxynucleotides (Abcam). A streptavidin-horseradish peroxidase (HRP) conjugate is used to detect biotinylated nucleotides and diaminobenzidine (DAB) subsequently reacts with the HRP-labeled cellular components and creates an insoluble brown substrate at the site of DNA fragmentation (Abcam). The Methyl Green counterstain allows the visualization of cells in the tissue sample. Cells that are pyknotic, mitotic, or apoptotic will exhibit an increased uptake of Methyl Green (Trevigen Inc., 2015).

4.5 Quantification of Glycosaminoglycan Concentration

The rate GAG degradation and synthesis were analyzed by measuring the concentration of sulfated GAGs (sGAG) in the tendon tissue digests and in the media of irradiated and non-irradiated samples using a dimethylmethelene blue (DMMB) assay.

Culture media (15 mL) was taken from all samples daily following irradiation for 5 days and stored in conical tubes at -20°C. Tendon tissue samples were taken 3 and 5 days after irradiation and were stored with 15mL of fresh media at -20°C until ready to use, at which time they were brought to room temperature in the water bath (37°C). A collagenase tissue digestion procedure was then performed on the tendon tissue samples. They were digested separately by category using a modification of a previously described method (Mazzocca et al., 2012) using bovine serum albumin (fraction V) in low-glucose DMEM and Collagenase Type I (Appendix I).

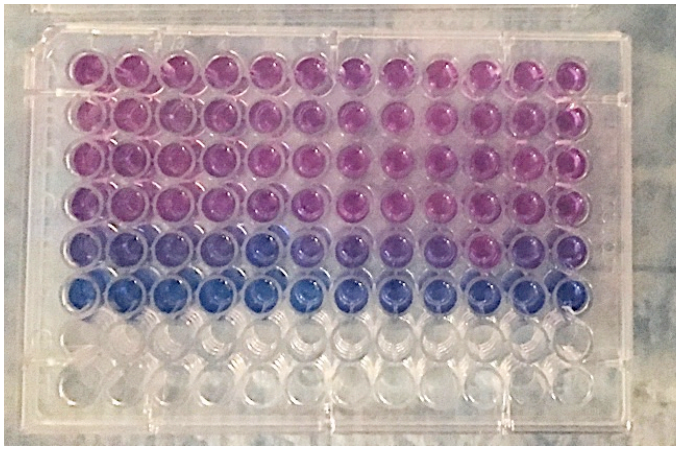

Figure 4.4: Plate for standard curve with increasing concentrations of chondroitin sulfate

Culture media and tissue digests were then tested for sGAG content using the dimethylmethelene blue (DMMB) assay (Appendix J). Using a 96-well plate, 200µL of dimethylmethylene blue was added to 20µL of each sample. The standard curve was created using increasing concentrations of chondroitin sulfate (Sigma-Aldrich) in order to determine a linear regression equation (Figure 4.4). Immediately, absorbance was read using a Synergy 4 microplate reader at 525nm (BioTek, Winooski, VT). The plate of the

microplate reader was programmed to shake slowly for five seconds prior to reading the absorbance. The sGAG content for each sample was determined by substituting the absorbance measurements into the linear regression equation given by the standard curve.

4.6 Statistics

For the Masson's Trichrome Stain, the RGB measurements were taken from a large pool of images taken of the slides (n = 20, 10 control samples and 10 irradiated samples) in order to quantify the staining of collagen (blue) and muscle, cytoplasm, and keratin (red). The readings for red and blue were averaged for each sample group to show a trend in the collagen content of the tissue samples. Student's *t*-tests were then used to test for significant variation between the means. For the DMMB assay, Student's *t*-tests were used to test for significance in GAG content of the media ($n = 24$) and tissue ($n = 27$).

4.7 References

Abcam. Product datasheet, *in situ* direct DNA fragmentation (TUNEL) assay kit ab66108.

Fischer, A. H., Jacobson, K. A., Rose, J., & Zeller, R. (2008). Hematoxylin and eosin staining of tissue and cell sections. *Cold Spring Harbor Protocols,* doi: 10.1101/pdb.prot4986

Mazzocca, A. D., Chowaniec, D., McCarthy, M. B., Beitzel, K., Cote, M. P., McKinnon, W., & Arciero, R. (2012). In vitro changes in human tenocyte cultures obtained

from proximal biceps tendon: Multiple passages result in changes in routine cell markers. *Knee Surgery, Sports Traumatology, Arthroscopy, 20*(9), 1666-72.

Takara Bio Inc. *Cartilage staining kit, cat. # MK310, v1009*

Trevigen, Inc. (2015). *TACS® 2 TdT-DAB in situ apoptosis detection kit, cat #: 4810-30-K*. Gaithersburg, MD.

University of Utah, Spencer S. Eccles Health Sciences Library (2016). *Surgical Pathology—Histology; Staining Manual—Connective Tissue.* Retrieved from http://library.med.utah.edu/

CHAPTER 5

RESULTS AND DISCUSSION

5.1 Histology Results

5.1.1 Hematoxylin & Eosin

Staining of the sections with hematoxylin and eosin revealed some signs of apoptosis in the tissue sections from the control samples on days 3 and 5 (Figure 5.1); however, there was clear morphological evidence of an increase in the occurrence of apoptosis in the irradiated samples on both days 3 and 5 (Figure 5.2 & 5.3). Further examination of the irradiated samples using oil immersion microscopy further confirmed the morphological evidence, showing nuclear condensation and nuclear blebbing (Figure 5.4).

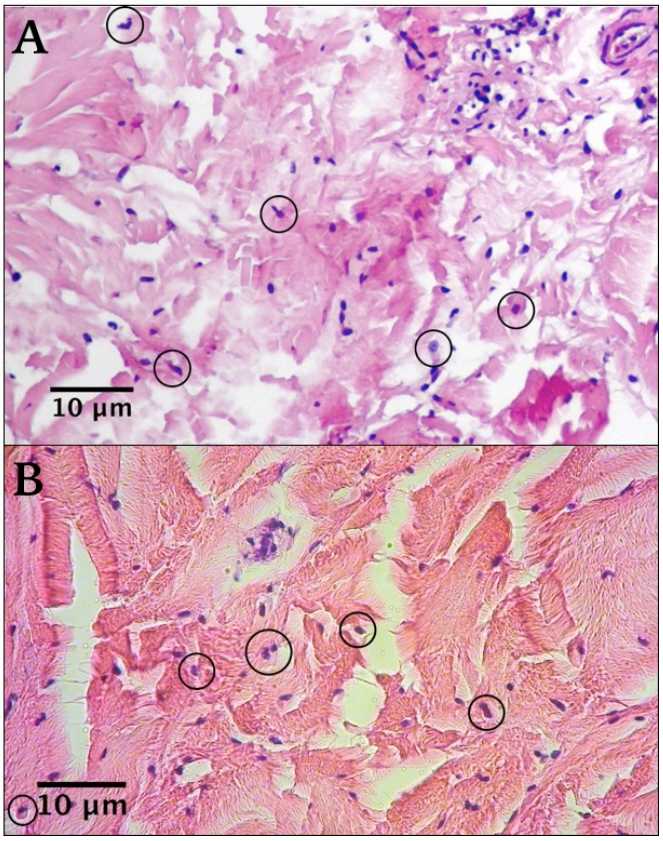

Figure 5.1: (A) Control sample, day 3, 200x; (B) Control sample, day 5; H & E Stain, 400x (cells displaying apoptotic characteristics are circled)

Figure 5.2: Irradiated tissue section (5Gy), 3 days post-radiation; H & E Stain, 400x (cells demonstrating characteristics of apoptosis are circled)

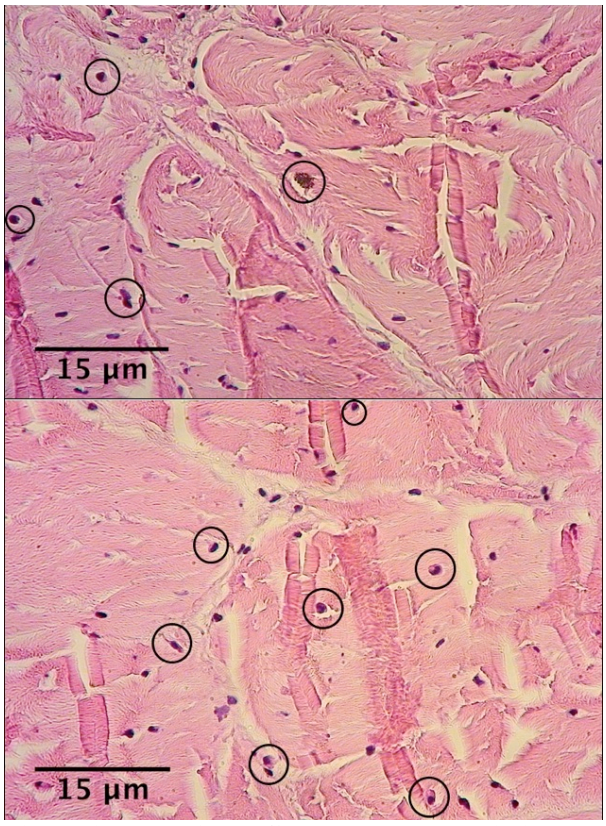

Figure 5.3: Irradiated tissue section (5Gy), 5 days post-radiation; H & E Stain, 400x (cells demonstrating characteristics of apoptosis are circled)

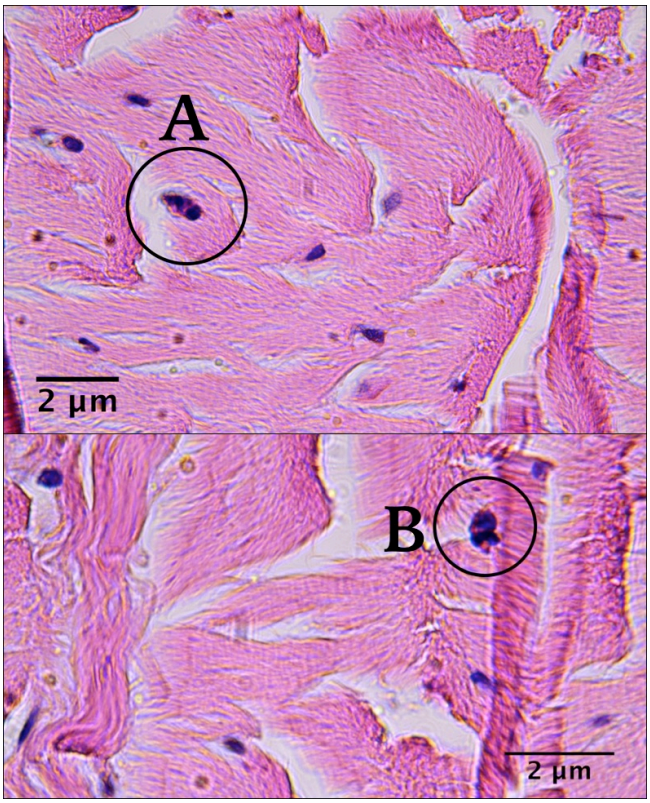

Figure 5.4: Examples of nuclear condensation (A) and nuclear blebbing (B); H & E Stain, 1000x (oil immersion), scale bars represent 2 µm.

5.1.2 Masson's Trichrome

Qualitatively, there appear to be slight variations between the control and irradiated samples upon observation following staining. Using ImageJ, RGB measurements were taken to quantify the amounts of red (muscle, cytoplasm, and keratin) and blue (collagen) staining in each image. These mean of these measurements was taken to provide an average to allow comparisons.

From visual observation of the non-irradiated control samples from day three (Figures 5.5 & 5.6), there appears to be an almost equal amount of red and blue dye. Using the RGB measurements from ImageJ, the overall blue-to-red ratio was calculated

to be 0.91, meaning that there was an almost equal distribution of the two dyes. By day five (Figures 5.7 & 5.8), the ratio of blue-to-red dropped to 0.54 for the control samples. From this data, we can see that the amount of cytoplasm, and/or keratin present surpasses the amount of collagen present between days 3 and 5. Qualitatively, the irradiated samples from day 3 show a distribution of red and blue similar to that of the control samples at day 3 (Figures 5.9 & 5.10). However, the blue-to-red ratio was calculated to be 0.85 (Table 5.1), which is less than the ratio of the control samples at day three. This means that there is slightly more cytoplasm, and/or keratin present in the irradiated samples than in the control samples after three days. Visual observation of the irradiated samples from day five appear to show a decrease in the amount of red staining (Figures 5.11 & 5.12). Conversely, the calculation of the blue-to-red ratio came to 0.75 (Table 5.1), meaning that there is still a greater amount of cytoplasm, and/or keratin than collagen present in the samples. A comparison between the differences in the blue-to-red ratios of the control and irradiated samples show that there is a greater difference between days three and five for the control samples than the irradiated ones (table 5.1). While there appeared to be difference, the quantified differences using ImageJ were not found to be statistically significant ($p > 0.05$).

Table 5.1: Comparison of the amount of red and blue stain for all samples.

	Red	Blue	Blue:Red	Difference (D3-D5)
0Gy D3	112.17	102.03	0.91	0.37
0Gy D5	155.36	83.65	0.54	
5Gy D3	104.84	88.64	0.85	0.09
5Gy D5	124.87	93.79	0.75	

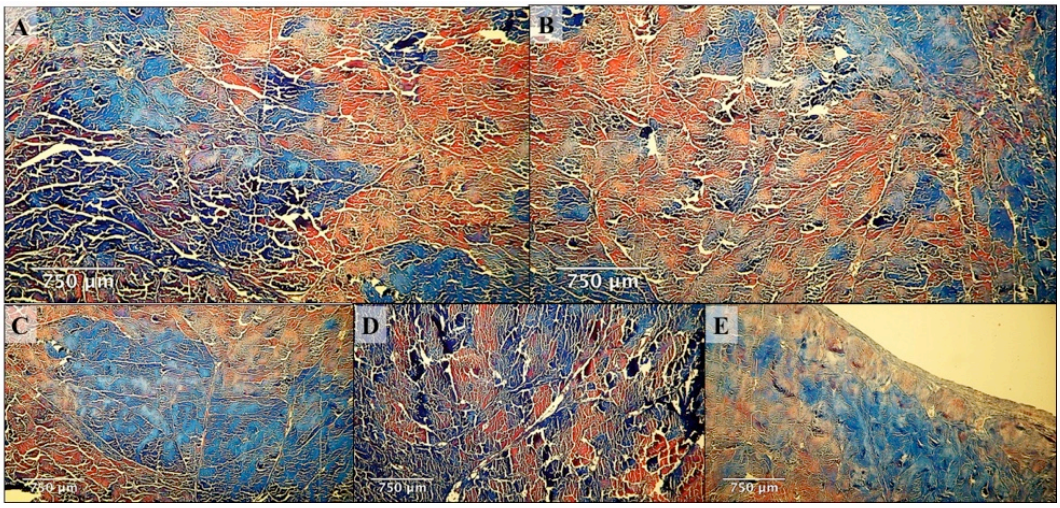

Figure 5.5: Examples of areas of control samples on day 3 which displayed more cytoplasm/keratin than collagen. Masson's Trichrome Stain, 40x, scale bars represent 750 µm

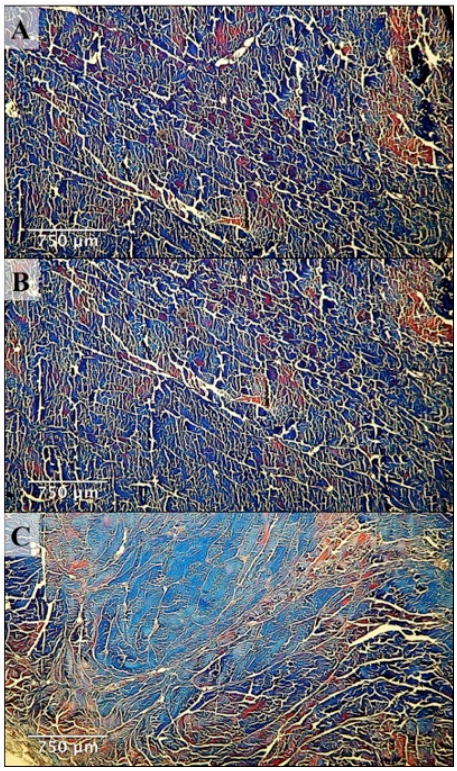

Figure 5.6: Examples of areas of control samples on day 3 which displayed more collagen than cytoplasm/keratin; Masson's Trichrome Stain, 40x, scale bars represent 750 µm

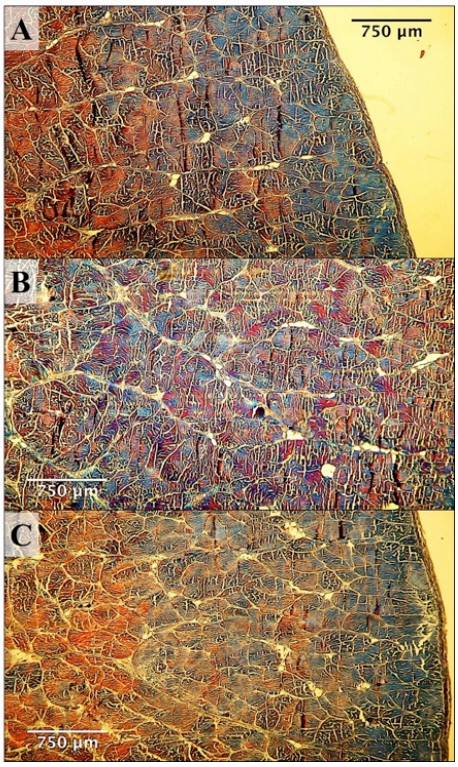

Figure 5.7: Examples of areas of control samples on day 5 which displayed more collagen than cytoplasm/keratin; Masson's Trichrome Stain, 40x, scale bars represent 750 µm

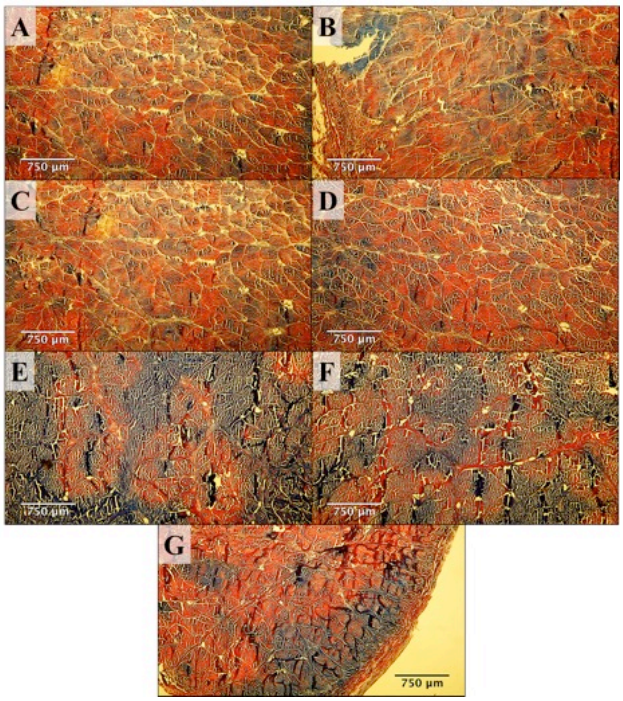

Figure 5.8: Examples of areas of control samples on day 5 which displayed more cytoplasm/keratin than collagen; Masson's Trichrome Stain, 40x, scale bars represent 750 µm

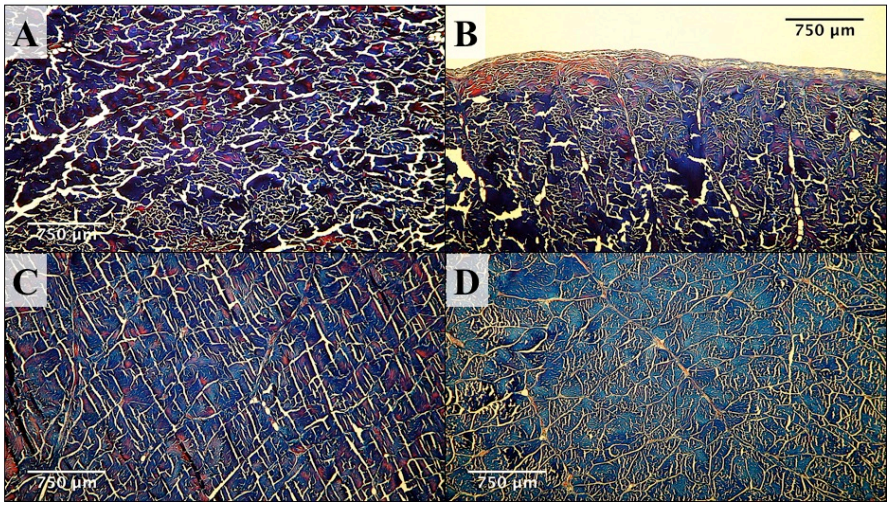

Figure 5.9: Examples of areas of irradiated samples on day 3 that displayed more collagen than cytoplasm/keratin; Masson's Trichrome Stain, 40x, scale bars represent 750 µm

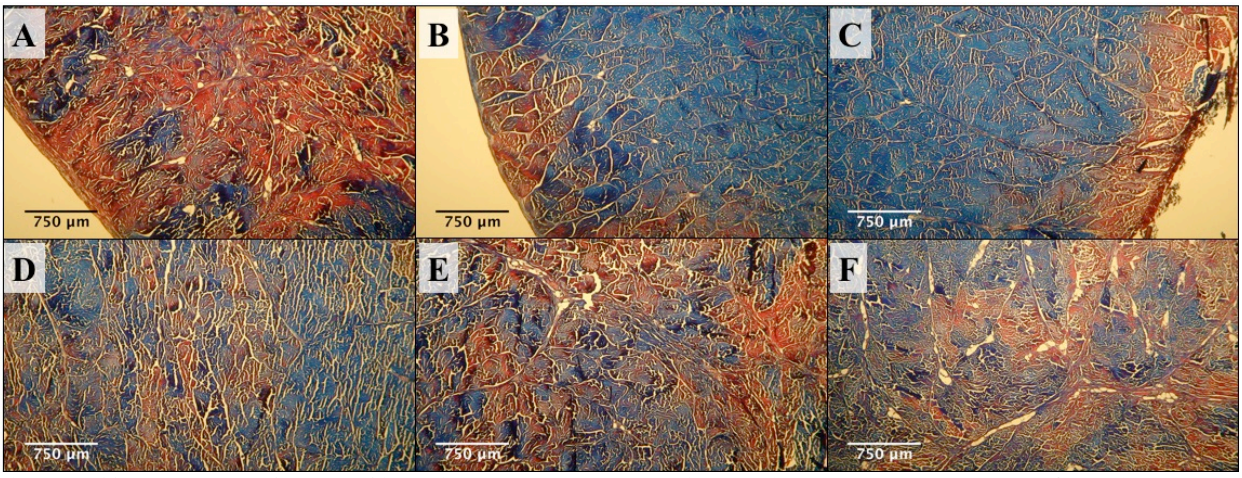

Figure 5.10: Examples of areas of irradiated samples on day 3 that displayed more cytoplasm/keratin than collagen; Masson's Trichrome Stain, 40x, scale bars represent 750 µm

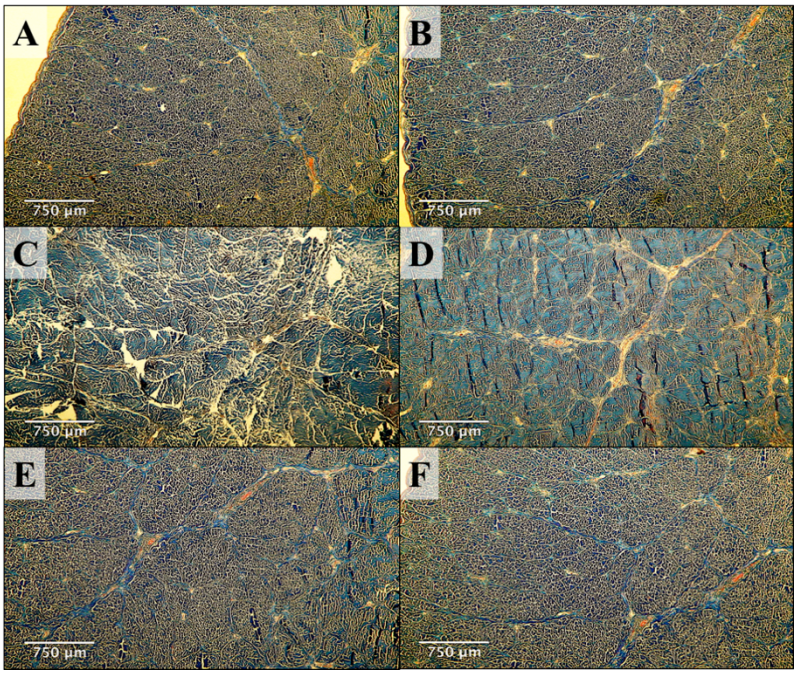

Figure 5.11: Examples of areas of irradiated samples on day 5 that displayed more collagen than cytoplasm/keratin; Masson's Trichrome Stain, 40x, scale bars represent 750 µm

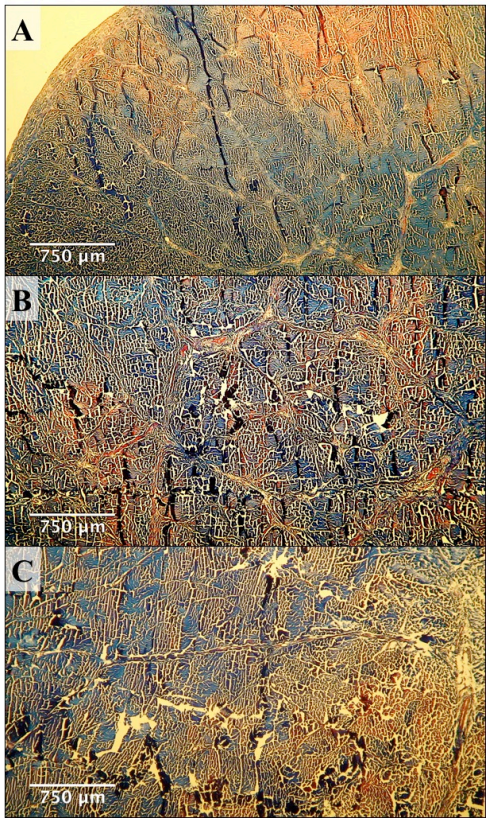

Figure 5.12: Examples of areas of irradiated samples on day 5 that displayed more cytoplasm/keratin than collagen; Masson's Trichrome Stain, 40x, scale bars represent 750 µm

5.1.3 Alizarin Red-S

There was evidence of an increase in Methyl Green uptake by the cells of the endotenon in the irradiated samples compared to the control samples (Figure 5.13). Furthermore, there were significantly more red spots indicative of calcium presence in the irradiated tissue sections on both day 5 when compared to the control samples from day 5

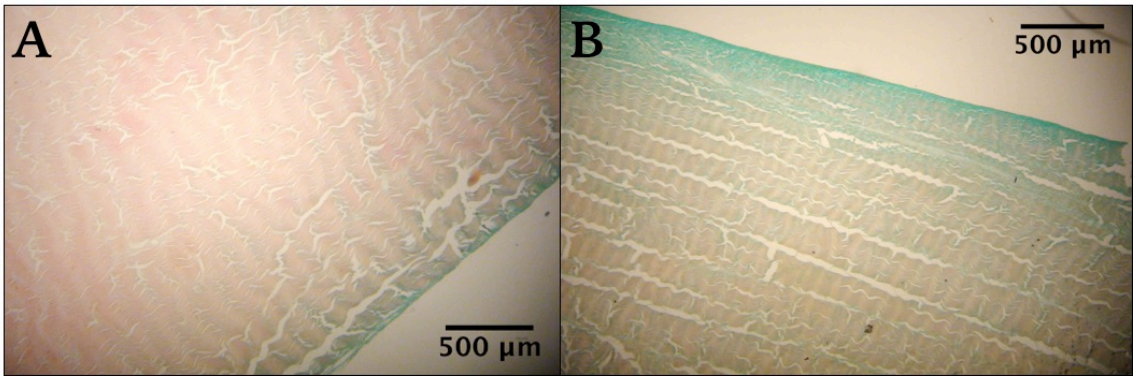

Figure 5.13: Increased methyl green uptake was seen in the endotenon of irradiated samples (B) compared to control samples (A); Alizarin Red S Stain, 40x, scale bars represent 500 µm

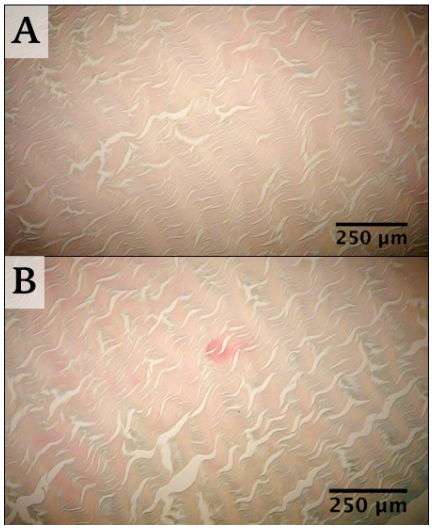

Figure 5.14: (A) Overall appearance of control tissue 5 days post-radiation, (B) Hardly any evidence of calcium was found in the control samples (red spot); Alizarin Red S Stain, 40x, scale bars represent 250 µm

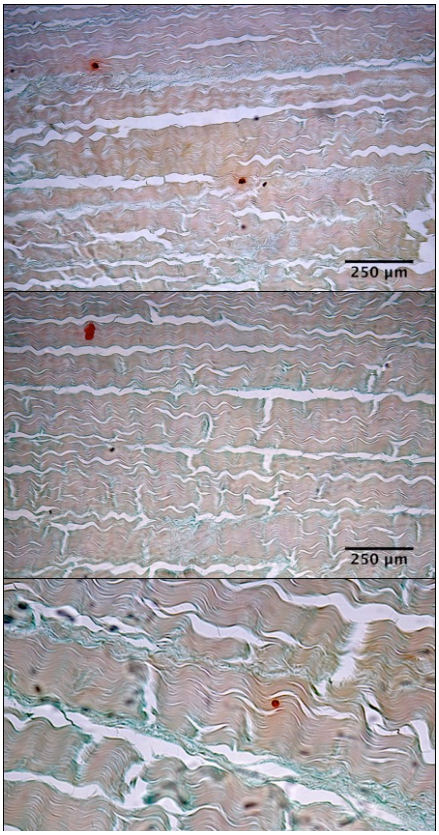

Figure 5.15: Irradiated tissue samples showing evidence of calcium deposits (red spots); Alizarin Red S Stain, 100x, scale bars represent 250 µm.

5.1.4 Safranin-O Staining

Staining of the tissue sections following the Safranin-O Staining protocol confirmed the morphological evidence of increased apoptosis in the irradiated tissues. As seen in Figure 5.16, there were morphological indicators of apoptosis, such as nuclear and cytoplasm condensation and nuclear blebbing, dispersed throughout the irradiated

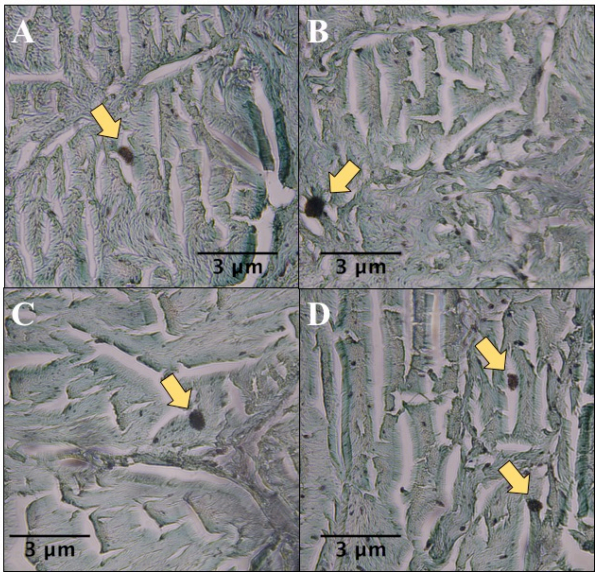

Figure 5.16: Irradiated tissue showed an increase in cellular apoptosis between day 3 (A&B) and day 5 (C&D) as indicated by the arrows; Saffranin-O Stain, 1000x (oil immersion), scale bars represent 3 µm

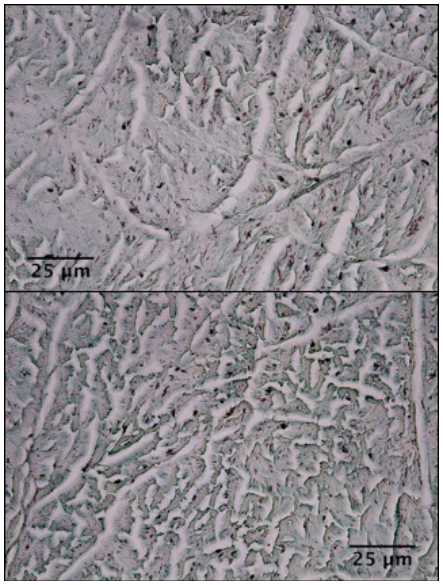

Figure 5.17: Samples showing overall appearance of control tissue samples on day 5; Saffranin-O Stain, 400x, scale bars represent 25 µm

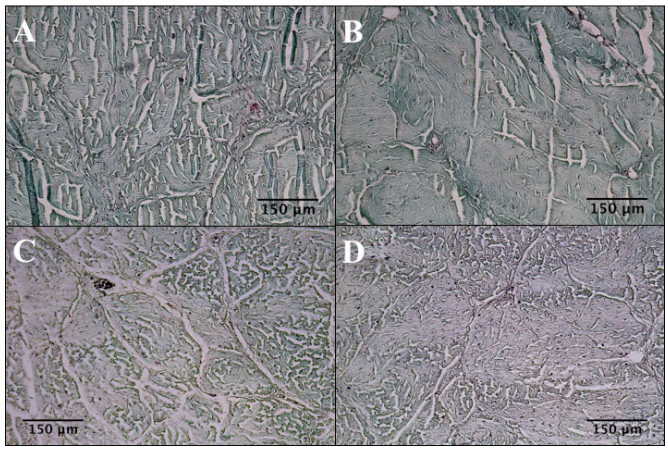

Figure 5.18: Irradiated tissue sections (A&B) showing decreased PG expression (orange areas) compared to control samples (C&D). 200x, scale bars represent 150 µm

tendon tissue. In contrast, most of the control tissue samples were similar to Figure 5.17 and didn't display an increased expression of apoptosis, although some apoptotic bodies were seen, owing to apoptosis being a normal cellular event.

Additionally, orange staining due to Safranin-O's affinity for PGs was observed to assess change in PG content. Upon observation, there was a decrease in orange staining in the irradiated tissue sections compared to the control sections (Figure 5.18), representative of a decrease in the presence of PGs in the irradiated tissue and potentially indicative of an increase in PG concentration in the culture media.

Additionally, orange staining due to Safranin-O's affinity for PGs was observed to assess change in PG content. Upon observation, there was a decrease in orange staining in the irradiated tissue sections compared to the control sections (Figure 5.18), representative of a decrease in the presence of PGs in the irradiated tissue and potentially indicative of an increase in PG concentration in the culture media.

5.2 *In Situ* Apoptosis Detection Results

With the assay that was used, DNA fragmentation is indicated by brown staining using DAB. In the control samples from days three and five, very little brown staining was observed (Figure 5.19, 5.20, & 5.21). In the irradiated samples on day three, there was a slight increase in cells displaying brown staining compared to the control samples (Figure 5.22). On day five, the irradiated samples displayed a substantial increase in brown staining (Figure 5.23), which is consistent with the morphological data obtained through H&E and Safranin-O staining. Furthermore, apoptotic cells are said to display an

increased uptake of Methyl Green and this was seen in comparison of the control and

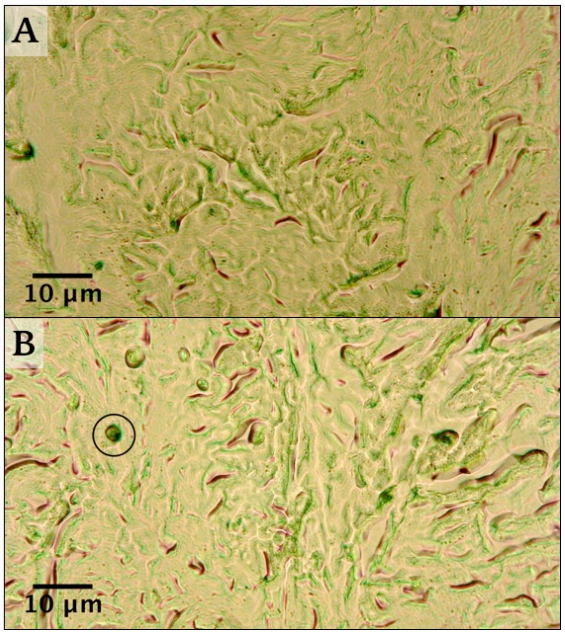

Figure 5.19: Control tissue samples on day 3; (A) General appearance of tissue, (B) Some signs of apoptosis were seen as identified by the circle; TACS ® 2 TdT-DAB *In Situ* Apoptosis Detection, 400x, scale bars represent 10 µm

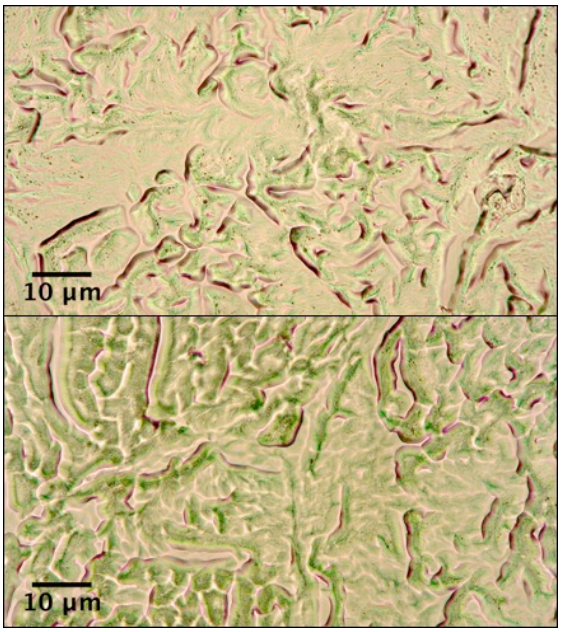

Figure 5.20: Overall appearance of control samples on day 5; TACS ® 2 TdT-DAB *In Situ* Apoptosis Detection, 400x, scale bars represent 10 µm

irradiated samples from days three and five.

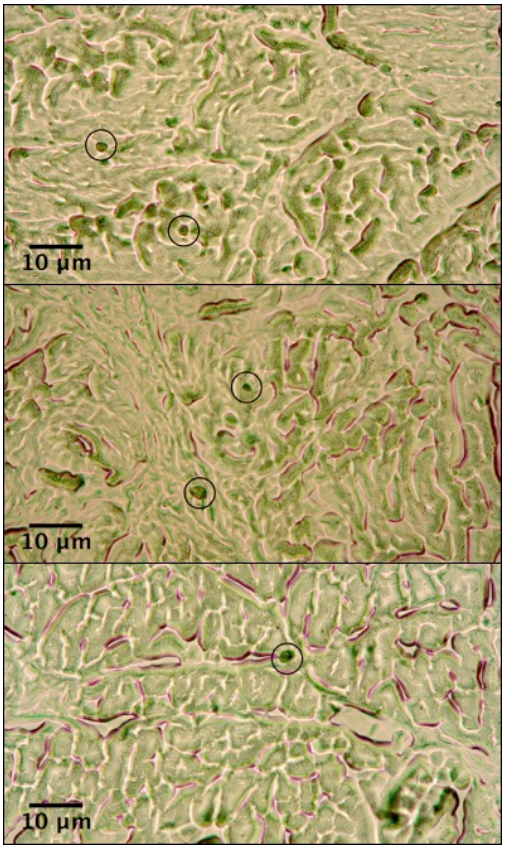

Figure 5.21: Control tissue samples on day 5, some signs of apoptosis were seen as indicated by the circles; TACS ® 2 TdT-DAB *In Situ* Apoptosis Detection, 400x, scale bars represent 10 µm

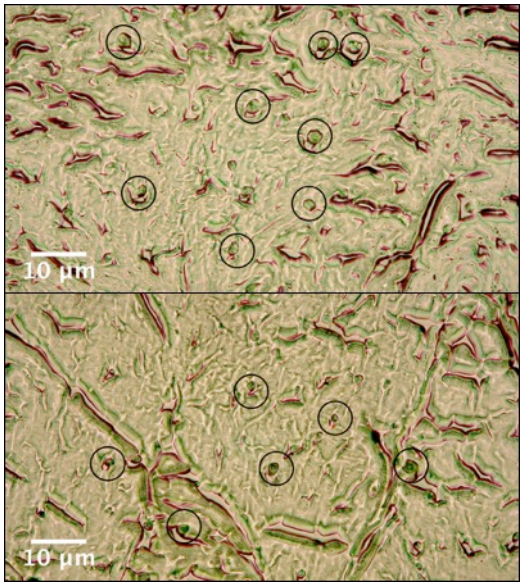

Figure 5.22: Irradiated tissue 3 days post-irradiation, increased apoptosis was observed as indicated by the circles; TACS ® 2 TdT-DAB *In Situ* Apoptosis Detection, 400x, scale bars represent 10 µm

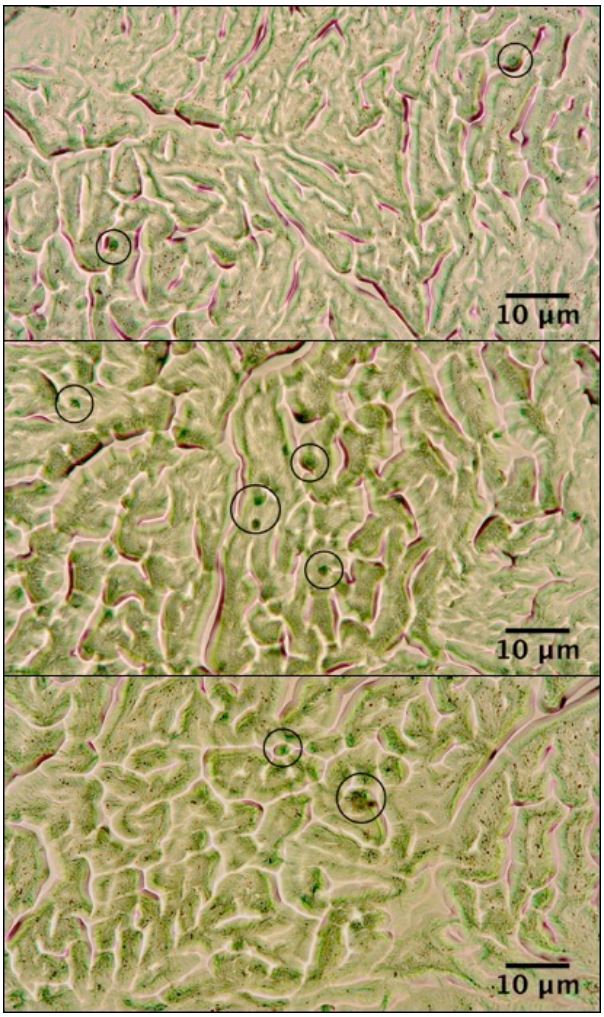

Figure 5.23: Irradiated tissue 5 days post-irradiation, increased apoptosis was observed as indicated by the circles; TACS ® 2 TdT-DAB *In Situ* Apoptosis Detection, 400x, scale bars represent 10 µm

5.3 Dimethylmethylene Blue Assay Results

The normal curve generated from the varying concentrations of CS in standard solution appeared to saturate at CS concentrations greater than 125 µg/mL (Figure 5.24). Therefore, only data from the three lowest concentrations (0 – 125 µg/mL) was used to calculate the average standard regression line (Figure 5.25).

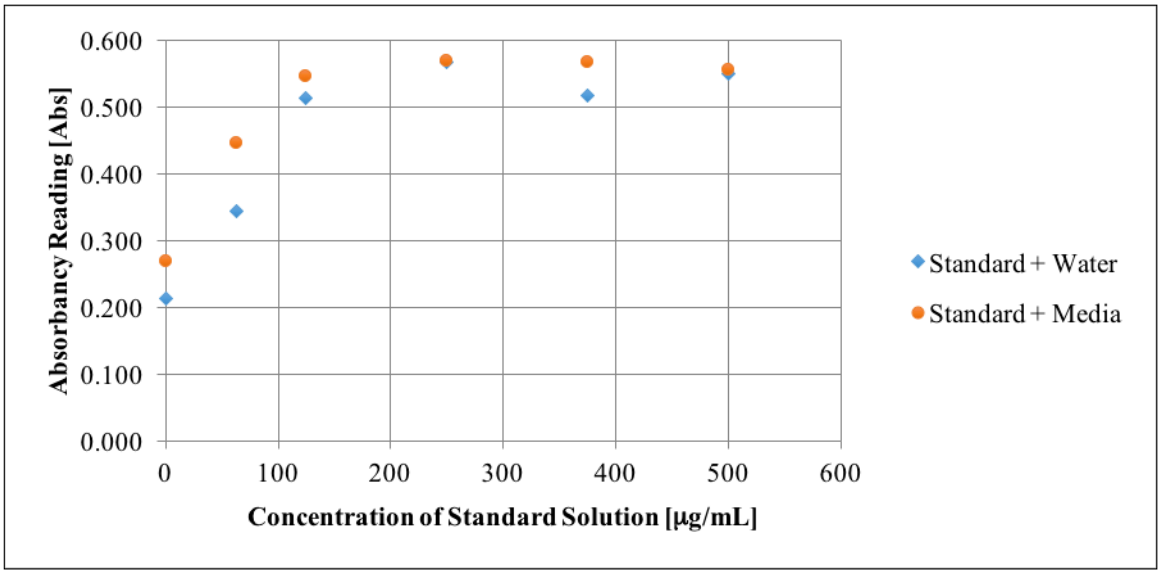

Figure 5.24: Normal Curve of DMMB Assay

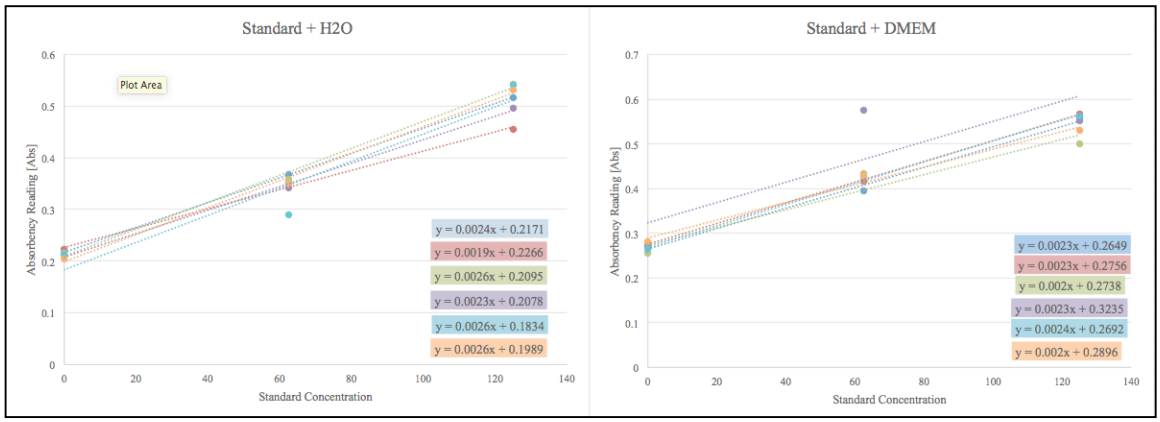

Figure 5.25: Averages of the regression lines on these two graphs were used to calculate an average regression line for normalization of the assay data

Three and five days following irradiation, the sGAG content in the irradiated tissue was noticeably lower than in the control tissue (Figure 5.26). This data coincides with the evidence introduced earlier from the Safranin-O staining showing less Safranin-O staining of PGs in the irradiated versus control samples. Student's t-test on the absorbency values averaged by tissue piece (n =27) showed statistical differences between the sGAG content in the irradiated tissue compared to the control samples on both days three and five (Figure 5.26).

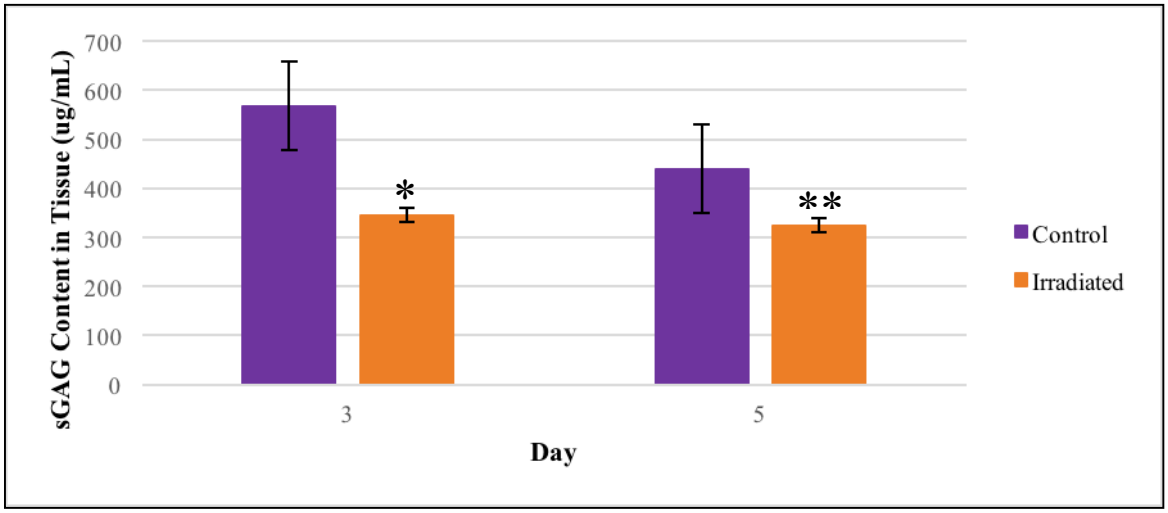

Figure 5.26: sGAG content in the tissue at three and five days after irradiation normalized to the standard curve. Irradiated samples had significantly lower sGAG content when compared to control samples on both days (*, $p < 0.01$, n =27; **, $p < 0.01$, n =27). Error bars indicate ±standard deviation.

Over the first four days, the sGAG content in the culture media of the control and irradiated samples showed very similar results. However, on day five, there was a significantly greater difference between the media of the control and irradiated samples (Figure 5.27). Results from Student's t-test on the absorbency readings from day five for both control and irradiated groups show significantly higher sGAG content in the culture

media of the irradiated sample than the culture media of the control samples ($p < 0.05$, $n = 6$) (Figure 5.28).

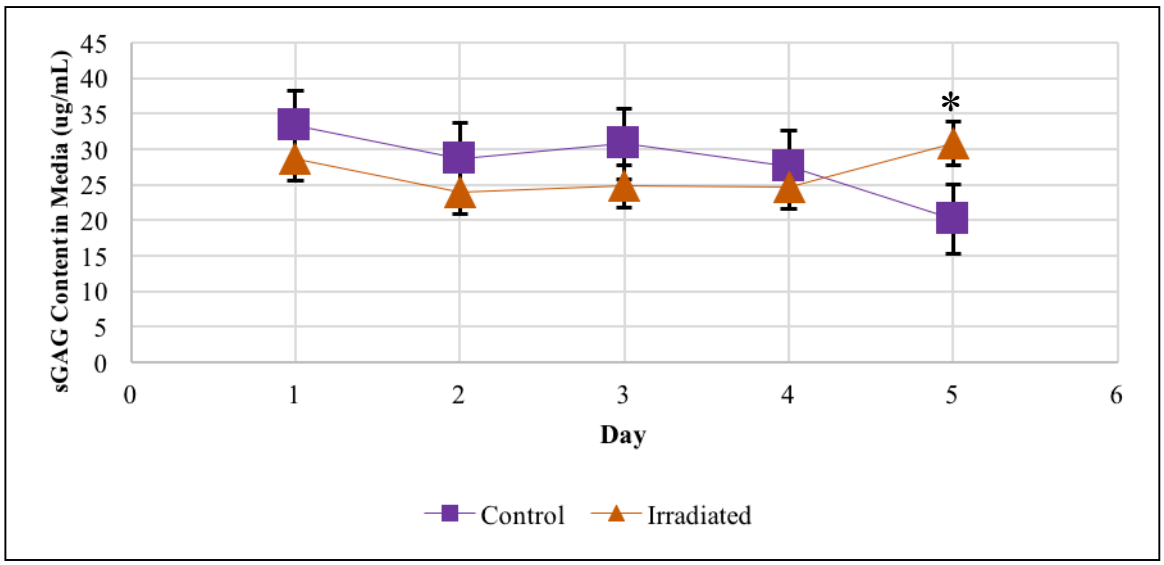

Figure 5.27: Normalized sGAG content in the culture media over time (n = 24). Significantly higher sGAG was released into the media in irradiated samples when compared to control samples at Day 5 (*, p < 0.01), Error bars indicate ±standard deviation.

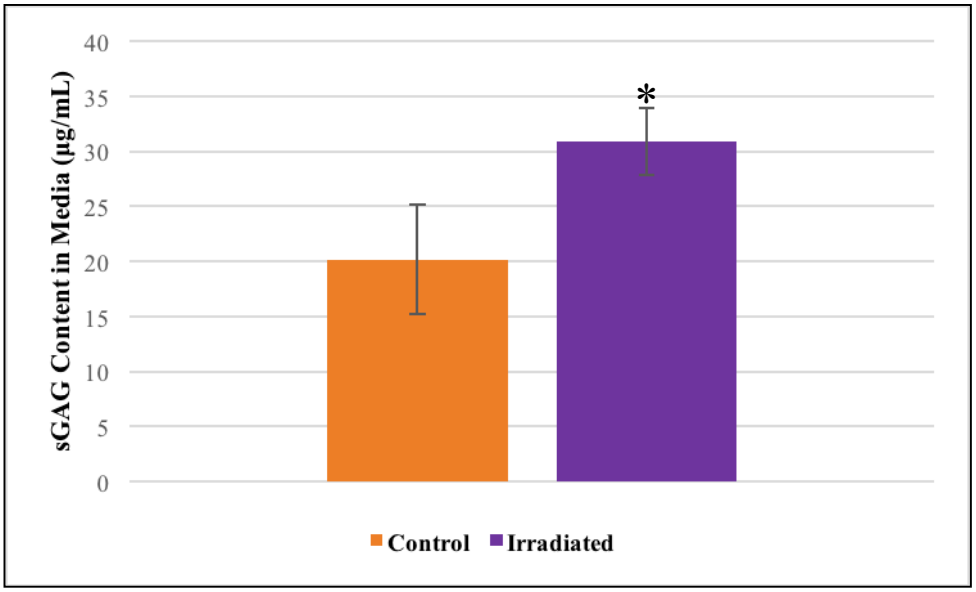

Figure 5.28: Normalized sGAG content in the culture media five days after irradiation. Culture media of the irradiated samples had significantly higher sGAG content when compared to control media on day 5 (*, p < 0.05, n =6). Error bars indicate ±standard deviation.

5.4 Discussion

Studies have shown that radiation is known to cause genomic instability (Morgan et al., 1996), leading to cellular death (Cohen-Jonathan et al., 1999; Grasl-Kraupp et al., 1995). Apoptotic cells are often seen following radiation in tissue sections. Results from the Hematoxylin and Eosin and Safranin-O staining methods revealed morphological data to support this. Results from the histological analysis suggest that there is an increase in the amount of cells undergoing apoptosis in irradiated tissue and this continues up to five days after irradiation. This conclusion was further supported by DNA fragment end labeling with DAB.

Based on the results seen from staining the tissue sections with Alizarin Red S, there appears to be an increase in the presence of calcium salts as a result of the radiation exposure. This indicates that γ radiation induces a slight calcification in the tendon tissue. This event has been shown to cause negative changes in tendon mechanical properties. For example, in the case of Achilles tendinitis, damaged tendon fibers thicken and calcify, or harden, causing tendons to adapt a limited range of motion accompanied by pain and swelling. Additionally, with interstitial Achilles tendinitis, bone spurs tend to form (American Academy of Orthopaedic Surgeons, 2016). Furthermore, although mechanical testing was not executed during this study, evidence of potential negative impact of the radiation on the mechanical properties of the tendon became evident during preparation for histological testing. While using the microtome to slice the tissue sections, the tissue would pull apart a great deal and for the Alizarin Red S stain, had trouble maintaining contact with the charged slides.

Results from the DMMB assay revealed that, for the irradiated sample group, there was a significant increase in sGAG concentration in the culture media on day five. The results also showed that there were significantly less sGAGs expressed in the irradiated tissue than in the control tissues on both days three and five following irradiation. Because GAGs are the side chains upon which PGs rely, the decrease in sGAGs in the tissue implies a decrease in the amount of PGs as well. Studies have shown that tendons deficient in certain PGs also show a decrease in strength and stiffness (Zhang et al., 2006).

Research has reported that tendons have a poor healing environment which is amplified by additional factors such as disease and prolonged immobilization (Lin et al., 2004). Therefore, it is possible that the tendons investigated in this study were ideal situation cases. In the case of radiotherapy patients, the tendons surrounding the tumor (for example, in the case of a tissue sarcoma in the shoulder) would be affected by those previously mentioned additional factors.

Research has also drawn a connection between oxidative changes caused by radiation and genomic instability in cells (Azzam et al., 2012). Furthermore, Sutherland et al. (2000) and Nikjoo et al. (1991) reported that approximately 60 ROS per nanogram of tissue are generated within less than a microsecond from a hit caused by 137-Cesium γ rays. It was reported that such a nuclear concentration of ROS could cause extensive oxidative injury in addition to causing modifications to normal biochemical reactions (Nikjoo, Goodhead, Charlton, & Paretzke, 1991; Sutherland, Bennett, Sidorkina, & Laval, 2000). The results from this study showed clear evidence of apoptosis and DNA

fragmentation. From this, we can conclude that potentially widespread oxidative changes are occurring in the irradiated tendons.

5.5 References

American Academy of Orthopaedic Surgeons. (2016). Achilles tendinitis. Retrieved from aaos.org

Azzam, E. I., Jay-Gerin, J. –P., & Pain, D. (2012). Ionizing radiation-induced metabolic oxidative stress and prolonged cell injury. *Cancer Letters, 327*, 48–60. Lin, T. W., Cardenas, L., & Soslowsky, L. J. (2004). Biomechanics of tendon injury and repair. *Journal of Biomechanics, 37*, 865-877.

Morgan, W. F., Day, J. P., Kaplan, M. I., McGhee, E. M., & Limoli, C. E. (1996). Genomic instability induced by ionizing radiation. *Radiation Research, 146*(3), 247-258.

Nikjoo, H., Goodhead, D. T., Charlton, D. E., & Paretzke, H. G. (1991). Energy deposition in small cylindrical targets by monoenergetic electrons. *International Journal of Radiation Biology, 60*, 739-756.

Sutherland, M., Bennett, P. V., Sidorkina, O., & Laval, J. (2000). Clustered DNA damages induced in isolated DNA and in human cells by low doses of ionizing radiation. *Proceedings of the National Academy of Sciences of the United States of America, 97*, 103-108.

Zhang, G., Ezura, Y., Chervoneva, I., Robinson, P. S., Beason, D. P., Carine, E. T., . . . Birk, D. E. (2006). Decorin regulates assembly of collagen fibrils and acquisition

of biomechanical properties during tendon development. *Journal of Cellular Biochemistry, 98*, 1436-1449.

CHAPTER SIX

CONCLUSIONS AND SUGGESTIONS FOR FUTURE WORK

6.1 Conclusions

A great deal of research has focused on the detrimental effects of ionizing radiation on biological tissues over the past few decades. However, while most of the studies involving ionizing radiation and tendinous tissues have dealt with high levels (kGy) of γ radiation, very few studies focus on the effects of low- and moderate-dose gamma irradiation on tendons. In this study, we sought to dose the tendons with 5 Gy of γ radiation in order to investigate the immediate effects of low dose radiation. The lower dosing is important to understand what happens to the tendon tissue in the few days following a dose of radiation treatment.

In the first phase of the study, histological aspects of the tendon were examined. Masson's Trichrome revealed an increased expression of collagen while H&E and Safranin-O found an increased occurrence of apoptosis which was confirmed by DNA fragment end-labeling.

The second phase of the study investigated the sGAG content of the tissue and culture media over time following irradiation exposure. Significant differences were seen between the control and irradiated groups in the sGAG content within the tissue (on days 3 and 5) and in the culture media (on day 5).

6.2 Next Steps and Suggestions for Future Studies

Due to the increase in collagen expression seen in the tissue sections stained with Masson's Trichrome and Safranin-O, further work should be done to determine the specific collagen types present. Pataridis et al (2008) described a method for identification of collagen types I-V in rat tissue in tissues using HPLC-MS/MS (High Performance/Pressure Liquid Chromatography-Tandem Mass Spectrometry coupled to an IT mass spectrometer)(Grebe & Singh, 2011). The method used in Pararidis' study is based on collagen fragmentation by cyanogen bromide following trypsin digestion. Then, analyses of resulting peptide mixtures, or peptide maps, were performed using HPLC-MS/MS. Peptides specific to each collagen type were selected; the peptides selected for this study are found in human, bovine, & rat collagens, allowing this to be applied to the tissues of other species. Pataridis also cites the most common method for determining total collagen is based on quantitation of hydroxyproline, which accounts for approximately 10% of the collagen molecule (Stagemann & Stalder, 1967; Verch, Wallach, & Peabody, 1979; Pødenphant, Larsen, Christiansen, 1984).

We developed a method for sample mounting and testing (Appendix K). However, due to material and time constraints, mechanical testing was not able to be carried out on our samples. Based on the morphological data from the tissue sections stained with Alizarin Red S, mechanical testing should reveal interesting results. Calcium deposits in tendons, as well as other connective tissues, have shown a negative correlation with biomechanical properties (Article from AAOS, find others). Additionally, Fideler et al. have reported a dose-dependent effect of irradiation on all

biomechanical parameters investigated in their study. The results indicated that there was a statistically significant ($p < 0.01$) reduction in maximum force, strain energy, modulus, and maximum stress of the human bone-patellar tendon-bone allografts after exposure to γ irradiation. Research reported by Danielson et al (1997) and Zhang et al (2006) describe a close correlation between the presence of decorin, a PG, and mechanical properties of the tissue. In our study, data obtained from the DMMB assay showed changes in the GAG content of the tissue and culture media of irradiated samples. Therefore, considering the results from our study showing evidence of calcium staining in irradiated tissues as well as the reduction in the tissue GAG content, it seems likely that irradiation at the doses used in this study could lead to a reduction of several of the tendon's mechanical properties.

Our results with the Safranin-O and DMMB assays show that 5Gy of γ radiation induces changes in the content of PGs (i.e. aggrecan) and sGAGs in the tendon tissue. Taking this into account, further experiments should be performed in order to measure the rate of PG deposition and turnover in tendinous tissue. Waggett et al (2004) described such an experiment, which they conducted on bovine digital flexor tendon explants. The explants were precultured, then cultured for an additional four days in two experimental groups. One group was given marimastat (0-2 μM) or acitonin (0-200 μM). Following the second culture, the explants were pulse-chase labelled with sulfate (^{35}S). The rate of turnover of ^{35}S-labelled PGs from the tendon matrix could then be calculated from the amount of ^{35}S-labelled macromolecules seen in the medium each day, and in the matrix of the explants at the end of the experiment's allotted time frame.

Along the same lines, an investigation into the types of PGs experiencing fluctuations in turnover rate is suggested. Zhang and colleagues published a similar study in 2006 in which they were able to indicate the presence or deficiency of the PGs decorin and biglycan in the tendons of mice. The results from the tissue samples stained with Safranin-O showed a decreased presence of PGs in the irradiated tissue, further confirming a change in PG turnover as a result of gamma radiation.

Future research on this topic should involve extending the length of the study well past five days following radiation exposure. Based on the results from the historical analyses and from the DNA fragmentation end-labeling assay, the length of the increase in apoptotic bodies present in the tendon tissue should be examined. Additionally, based on the data gathered from the DMMB assay, extending the length of the study would allow investigators to determine if there is a further increase in the sGAG content of the culture media and if the decreased expression in the tissue returns to levels similar to the control tendon over time. Extending the study duration could help to determine whether the changes in tendon matrix observed in this study were short-term effects and can be reversed or whether they persist over longer periods. In addition, further studies into other clinically relevant dosage schemes and other types of radiation on tendinous tissue should be executed.

6.3 References

American Academy of Orthopaedic Surgeons. (2016). Achilles tendinitis. Retrieved from aaos.org

Fideler, B. M., Vangsness, C. T. J., Lu, B., Orlando, C., & Moore, T. (1995). Gamma irradiation: Effects on biomechanical properties of human bone-patellar tendon-bone allografts.*American Journal of Sports Medicine, 23*(5), 643-646.

Grebe, S. K. G., & Singh, R. J. (2011). LC-MS/MS in the clinical laboratory – where to from here? *The Clinical Biochemist Reviews, 32*(1)

Lin, T. W., Cardenas, L., & Soslowsky, L. J. (2004). Biomechanics of tendon injury and repair. *Journal of Biomechanics, 37*, 865-877.

Nikjoo, H., Goodhead, D. T., Charlton, D. E., & Paretzke, H. G. (1991). Energy deposition in small cylindrical targets by monoenergetic electrons. *International Journal of Radiation Biology, 60*, 739-756.

Pataridis, S., Eckhardt, A., Mikulikova, K., Sedlakova, P., & Miksik, I. (2008). Identification of collagen types in tissues using HPLC-MS/MS. *Journal of Separation Science, 31*, 3483-3488.

Pødenphant, J., Larsen, N. E., & Christiansen, C. (1984). An easy and reliable method for determination of urinary hydroxyproline. *Clinica Chimica Acta, 142*, 145-148.

Stegemann, H., & Stalder, K. (1967). Determination of hydroxyproline. *Clinica Chimica Acta, 18*, 267-273.

Sutherland, M., Bennett, P. V., Sidorkina, O., & Laval, J. (2000). Clustered DNA damages induced in isolated DNA and in human cells by low doses of ionizing

radiation. *Proceedings of the National Academy of Sciences of the United States of America, 97*, 103-108.

Verch, R. L., Wallach, S., & Peabody, R. A. (1979). Automated analysis of hydroxyproline with elimination of non-specific reacting substances. *Clinica Chimica Acta, 96*, 125-130.

Waggett, A. D., Rees, S. G., & Caterson, B. (2004). Increased turnover of proteoglycan aggregates in tendon *vs*. cartilage. *International Journal of Experimental Pathology, 85*(4), A76-A77.

Zhang, G., Ezura, Y., Chervoneva, I., Robinson, P. S., Beason, D. P., Carine, E. T., . . . Birk, D. E. (2006). Decorin regulates assembly of collagen fibrils and acquisition of biomechanical properties during tendon development. *Journal of Cellular Biochemistry, 98*, 1436-1449.

APPENDICES

APPENDIX A

Anti-Microbial Wash Protocol

Materials:

PBS -------- 500 mL
5 mM Benzamidine-hydrocholoride -------- 2.5 mL
2 mM phenylsulfonyl fluoride -------- 0.06 mL
Protease inhibitor cocktail -------- 1 mL
5 mM EDTA -------- 0.7306 g
5 mM N-ethyhnaleimide -------- 0.3128 g

Directions:

Place tendon sections in sample cups according to testing group (control & irradiated). Add enough anti-microbial wash to fully submerge all samples. Leave at room temperature for 20 minutes. After 20 minutes, remove samples from cups and wash with culture media (Appendix B).

Protocol adapted from:

Fukuta, S., Oyama, M., Kavalkovich, K., Fu, F. H., & Niyibizi, C. (1998). Identification of types II, IX and X collagens at the insertion site of the bovine achilles tendon. *Matrix Biology, 17*, 65-73.

APPENDIX B

Culture Media for Tendon Tissue Protocol

Materials:

1. Low glucose Dulbecco's Modified Eagles Medium (add 435 mL to make 500 mL media)
2. Fetal Bovine Serum: 10% v/v (50 mL/500 mL media)
3. Nonessential Amino Acids: 1% v/v (5 mL/500 mL media)

Directions:

1. Bring all ingredients to room temperature in warming bath.
2. Add FBS and Nonessential AA to DMEM.
3. Mix by inversion and store at 20°C (fridge temp).

APPENDIX C

Hematoxylin & Eosin (H&E) Staining Protocol

Fixation: Any
Technique: Paraffin or frozen

SOLUTIONS: Mix thoroughly before dispensing.

Hematoxylin I (Richard-Allan, Order # 7221)
Clarifier I (Richard-Allan, Order # 7401)
Bluing Reagent (Richard-Allan, Order # 7301)
Eosin-Y with Phloxine (Richard-Allan, Order # 71304)

STAINING PROCEDURE:

1.	Xylenes	10 dips
2.	Xylenes	5 min
3.	100% ETOH	10 dips
4.	100% ETOH	1 min
5.	95% ETOH	10 dips
6.	95% ETOH	1 min
7.	Tap Water	Till “sheeting” action occurs
8.	Distilled Water	1 min
9.	Hematoxylin	5 – 10 min (check with microscope)
10.	Tap Water	Till clear
11.	Clarifier	3 – 6 dips
12.	Tap Water	Till “sheeting” action occurs
13.	Bluing Reagent	1 min
14.	Tap Water	1 min
15.	95% ETOH	10 dips
16.	Eosin	30 – 45 sec
17.	95% ETOH	10 dips
18.	95% ETOH	10 dips
19.	100% ETOH	10 dips
20.	100% ETOH	1 min
21.	100% ETOH	3 min
22.	Xylenes	10 dips
23.	Xylenes	5 min

Let slides remain in last container until a coverslip is applied.

RESULTS:

Nuclei----------blue
Erythrocytes and eosinophilic granules----------bright pink to red
Cytoplasm and other tissue elements----------various shades of pink

Source: Richard-Allan Scientific™

APPENDIX D

Masson's Trichrome Protocol

Description: This method is used for the detection of collagen fibers in tissues such as skin, heart, etc. on formalin-fixed, paraffin-embedded sections, and may be used for frozen sections as well. The collagen fibers will be stained blue and the nuclei will be stained black and the background is stained red.

Fixation: 10% formalin or Bouin's solution
Section: paraffin sections at 5 μm

Solutions and Reagents:

Bouin's Solution**:**
Picric acid (saturated) ---------- 75 mL
Formaldehyde (37-40%) ---------- 25 mL
Glacial acetic acid ---------- 5 mL
Mix well. This solution will improve Masson Trichrome staining quality.

Weigert's Iron Hematoxylin Solution:

Stock Solution A:
Hematoxylin ---------- 1 g
95% Alcohol ---------- 100 mL

Stock Solution B:
29% Ferric chloride in water --------- 4 mL
Distilled water ---------- 95 mL
Hydrochloric acid, concentrated ---- 1 mL

Weigert's Iron Hematoxylin Working Solution:
Mix equal parts of stock solution A and B. This working solution is stable for 3 months (no good after 4 months)

Biebrich Scarlet-Acid Fuchsin Solution:
Biebrich scarlet, 1% aqueous --------- 90 mL
Acid fuchsin, 1% aqueous ----------10 mL
Acetic acid, glacial ---------- 1 mL

Phosphomolybdic-Phosphotungstic Acid Solution:
5% Phosphomolybdic acid ---------- 25 mL
5% Phosphotungstic acid ---------- 25 mL

Aniline Blue Solution:

Aniline blue ---------- 2.5 g
Acetic acide, glacial ---------- 2 mL
Distilled water ---------- 100 mL

1% Acetic Acid Solution:

Acetic acid, glacial ---------- 1 mL
Distilled water ---------- 99 mL

Procedure:

1. Deparaffinize and rehydrate through 100% alcohol, 95% alcohol 70% alcohol.
2. Wash in distilled water.
3. For Formalin fixed tissue, re-fix in Bouin's solution for 1 hour at 56 C to improve staining quality although this step is not absolutely necessary.
4. Rinse running tap water for 5-10 minutes to remove the yellow color.
3. Stain in Weigert's iron hematoxylin working solution for 10 minutes.
4. Rinse in running warm tap water for 10 minutes.
5. Wash in distilled water.
6. Stain in Biebrich scarlet-acid fuchsin solution for 10-15 minutes. Solution can be saved for future use.
7. Wash in distilled water.
8. Differentiate in phosphomolybdic-phosphotungstic acid solution for 10-15 minutes or until collagen is not red.
9. Transfer sections directly (without rinse) to aniline blue solution and stain for 5-10 minutes. Rinse briefly in distilled water and differentiate in 1% acetic acid solution for 2-5 minutes.
10. Wash in distilled water.
11. Dehydrate very quickly through 95% ethyl alcohol, absolute ethyl alcohol (these step will wipe off Biebrich scarlet-acid fuchsin staining) and clear in xylene.
12. Mount with resinous mounting medium.

Results:

Collagen ---------- blue
Nuclei ---------- black
Muscle, cytoplasm, keratin ---------- red

Positive Controls:

Skin, lung, stomach, intestine.

APPENDIX E

Saffranin-O Staining Protocol

Description: This method is used for the detection of cartilage, mucin, and mast cell granules on formalin-fixed, paraffin-embedded tissue sections, and may be used for frozen sections as well. The cartilage and mucin will be stained orange to red, and the nuclei will be stained black. The background is stained bluish green.

Fixation: Formalin fixed, paraffin embedded sections.

Solutions and Reagents:

Weigert's Iron Hematoxylin Solution:

Stock Solution A:
Hematoxylin ---------- 1 g
95% Alcohol ---------- 100 mL
Stock Solution B:
29% Ferric chloride in water ---------- 4 mL
Distilled water ---------- 95 mL
Hydrochloric acid, concentrated ---- 1mL

Weigert's Iron Hematoxylin Working Solution:
Mix equal parts of stock solution A and B. This working solution is stable for about 4 weeks.

0.05% Fast Green (FCF) Solution:
Fast green, FCF, C.I. 42053 ---------- 0.5 g
Distilled water ---------- 1000 mL

1% Acetic Acid Solution:
Acetic acid, glacial ---------- 1 mL
Distilled water ---------- 99 mL

0.1% Safranin O Solution:
Safranin O, C.I. 50240 ---------- 0.1 g
Distilled water ---------- 100 mL

Procedure:

1. Deparaffinize and hydrate slides to distilled water.
2. Stain with Weigert's iron hematoxylin working solution for 10 minutes.
3. Wash in running tap water for 10 minutes.
4. Stain with fast green (FCF) solution for 5 minutes.
5. Rinse quickly with 1% acetic acid solution for no more than 10 –15 seconds.

6. Stain in 0.1% safranin O solution for 5 minutes.
7. Dehydrate and clear with 95% ethyl alcohol, absolute ethyl alcohol, and xylene, using 2 changes each, 2 minutes each.
8. Mount using resinous medium.

Results:
Nuclei ---------- black
Cytoplasm ---------- bluish green
Cartilage, mucin, mast cell granules ---------- orange to red

APPENDIX F

Alizarin Red Staining Protocol

I. Stains

A. 1% Alizarin Red S Solution (Stable for ~1 Month)

1. Add 1 g alizarin red S to 100 ml distilled water
2. Add 10 ml 0.1% ammonium hydroxide to alizarin red solution with constant stirring. Resulting pH of stain should be 6.36-6.40. Make ammonium hydroxide solution by adding 0.1 ml ammonium hydroxide (C.P. 28%) to 100 ml distilled water.

B. 1% Light Green Solution

1. Add 1 g light green, SF yellowish to 100 ml distilled water.
2. Add 1 ml glacial acetic acid

II. Staining Procedure

A. Fix cells in 2% FA, 10 minutes, RT
B. Rinse with PBS several times
C. Add alizarin red S solution for 5-10 minutes
D. Remove excess stain with 5-6 changes of distilled water.
E. Counterstain in light green solution for ~8-10 seconds.
F. Immediately rinse off excess light green solution.
G. Keep in water.

APPENDIX G

TACS ® 2 TdT-DAB In Situ Apoptosis Detection Kit Protocol

(Trevigen Inc., Gaithersburg, MD; Catalog# 4810-30-K)

I. Materials Supplied:

Component:	Quantity:	Storage:
Proteinase K Solution	50 µL	-20 °C
Cytonin™	6 mL	4 °C
10X TdT Labeling Buffer	100 mL	4 °C
10X TdT Stop Buffer	100 mL	4 °C
TdT dNTP Mix	35 µL	-20 °C
TdT Enzyme	35 µL	-20 °C
Strep-HRP	30 µL	4 °C
DAB Solution	3.75 mL	- 20 °C
DAB Enhancer	1 mL	- 20 °C
50X Co_{2+}	30 µL	- 20 °C
50X Mg_{2+}	30 µL	- 20 °C
50X Mn_{2+}	50 µL	- 20 °C
TACS-Nuclease™	15 µL	- 20 °C
TACS-Nuclease Buffer	1.5 mL	4 ° C
1% Methyl Green	50 mL	RT

II. Materials and Equipment needed but not supplied:

Equipment

1. 1 - 20 µL, 20 - 200 µL, and 200 - 1000 µL pipettors
2. 37°C Incubator
3. 50 and 500 mL Graduated cylinders
4. 2 Coplin jars
5. -20°C and 4°C storage
6. Ice bucket
7. Standard light microscope
8. Cryostat or microtome
9. Humidity chamber
10. 57 °C incubator or slide warmer
11. Pipette helper
12. Timer

Reagents

1. Apoptosis Grade™ Water
2. 10X PBS
3. 37% Formaldehyde
4. Xylenes
5. 30% Hydrogen peroxide
6. 95% and 100% Ethanol (or denatured alcohol)
7. Methanol
8. Butanol
9. Mounting medium or alternative mounting solution e.g. Permount

Disposables

1. Treated Glass Microscope Slides (or alternative support)

2. 50 ml tubes
3. 1 - 200 µL and 200 - 1000 µL pipette tips
4. microcentrifuge tubes
5. 1.5 and 10 ml serological pipets
6. gloves
7. Hydrophobic Coverslips (optional)
8. Glass coverslips

III. Reagent Preparation:

Note: Reagents labeled with an asterisk (*) should be prepared immediately before use
(This is an abbreviated list, full reagent preparation can be found in the product manual on the Trevigen website: https://www.trevigen.com/docs/protocol_4810-30-K.pdf?guid=1455824221)

1. *** 3.7% Buffered Formaldehyde**

   50 mL of freshly prepared fixative is used to process 1 to 10 samples. To prepare, add:

37% Formaldehyde	5 mL
10X PBS	5 mL
ddH_2O	40 mL

   Wear gloves and exercise caution when handling formaldehyde solutions.

2. *** Proteinase K Solution**

   Use 50 µL of Proteinase K Solution per sample. Store on ice. Thaw provided Proteinase K at room temperature, then place on ice. To prepare, add:

	2 samples	10 samples	*n* samples
Deionized water	100 µL	500 µL	*n* x 50 µL
Proteinase K	2 µL	10 µL	*n* x 1 µL

3. *** Quenching Solution**

   Use 50 mL of Quenching Solution to process 1 to 10 samples. To prepare, add:

Methanol	45 mL
30% Hydrogen Peroxide	5 mL

4. **1X TdT Labeling Buffer**

   Dilute the 10X TdT Labeling Buffer (Cat# 4810-30-02) to 1X using distilled water. Leave at room temperature until use. Use 50 mL of 1X Labeling Buffer to process 1 to 10 samples. Remove an aliquot of 50 µL per sample or preparing the Labeling Reaction Mix (see below) and place on ice.

5. *** Labeling Reaction Mix**

   Thaw TdT dNTP Mix at room temperature, then place on ice. To maintain optimal enzyme activity, remove the TdT Enzyme tube from freezer only long enough to pipette the required volume. Alternatively, place the TdT Enzyme in a -20 °C freezer block. Prepare the Labeling Reaction Mix just before use and keep the prepared reaction mix on ice. Prepare 50 µL per sample in the sequence given below:

	2 samples	10 samples	*n* samples
TdT dNTP Mix	2 µL	10 µL	*n* x 1 µL
TdT Enzyme	2 µL	10 µL	*n* x 1 µL
50X Cation Stock	2 µL	10 µL	*n* x 1 µL
1X TdT Labeling Buffer	100 µL	500 µL	*n* x 50 µL

6. **1X TdT Stop Buffer**
   Dilute the 10X TdT Stop buffer to 1X using distilled water. Leave at room temperature until use. Use 50 mL of 1X TdT Stop Buffer to process 1 to 10 samples.

7. *** Strep-HRP Solution**

   Use 50 µL of Strep-HRP Solution per sample. Store at room temperature until use. To prepare, add:

	2 samples	10 samples	*n* samples
1X PBS	100 µL	500 µL	*n* x 50 µL
Strep-HRP	2 µL	10 µL	*n* x 1 µL

8. *** DAB Solution**

   Thaw DAB at 37 °C for 30 min. If not using the full bottle, store the remaining stock solution back at -20°C. It is not recommended to freeze thaw DAB stock solution more than three times. If required, aliquot in smaller volume and store at -20°C protected from light. To prepare, add:

1X PBS	50 mL
DAB	250 µL
DAB Enhancer	0 to 50 µL
30% Hydrogen Peroxide	50 µL

   Use only fresh 30% hydrogen peroxide. It is recommended that 6 mL aliquots of fresh 30% hydrogen peroxide are made and stored at 4 °C. For each labeling procedure use a fresh 30% hydrogen peroxide aliquot then discard any remaining solution.
   Note: Do not place the DAB (Cat# 4800-30-07) on ice after thawing, otherwise the DAB will precipitate. Prepare DAB Solution no more than 30 minutes before use. Use 50 mL of DAB Solution to process 1 to 10 samples. DAB Enhancer may be used to intensify and darken DAB staining; the concentration must be optimized experimentally.

IV. Sample preparation and fixation:

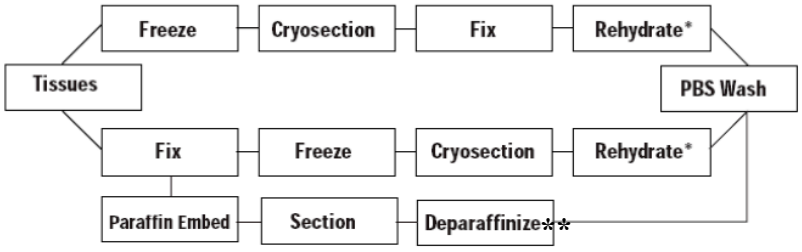

Figure 3: Tissue sample preparation flow chart, taken from TACS(R) TdT-DAB In Situ Apoptosis Detection Kit Protocol

****** Deparaffinization: Sections prepared from paraffin blocks require removal of the paraffin prior to the labeling reaction.

Method:

1. Warm slides to 57 °C for 5 minutes.
2. Immerse sections in 2 changes of xylenes, 5 minutes each.
3. Immerse sections in 100%, 95% then 70% ethanol, 5 minutes each.
4. Wash 2 times in 1X PBS, 5 minutes each.
5. Proceed to Labeling Procedure below.

V. Labeling Procedure for Immobilized, Fixed, and Rehydrated Samples in 1X PBS

Step	Instructions	Notes
1	Place samples in 1X PBS for 10 minutes at room temperature after rehydration in ethanols. Carefully dry glass slide around sample.	DO NOT allow sample to DRY at any stage prior to completion of protocol.
2	Cover sample with 50 µL of Proteinase K Solution and incubate 15 to 30 minutes at room temperature, or cover sample with 50 µL of Cytonin™ and incubate for 30-120 minutes at room temperature or 4 °C. If necessary, use Cover Slips.	Cytonin™ is recommended for frozen sections and when protease treatment will destroy antigens of interest in double labeling experiments. Time of Proteinase K treatment will vary between cell type. Start at 15 minutes and increase if no labeling occurs.
3	Wash 2 times in deionized water, 2 minutes each.	
4	Immerse slides in Quenching Solution for 5 minutes at room temperature.	Do not leave longer than 5 minutes since hydrogen peroxide can damage DNA.
5	Wash samples in 1X PBS for 1 minute at room temperature.	

6	Immerse slides in 1X TdT Labeling Buffer for 5 minutes.	
7	Cover sample with 50 µL of Labeling Reaction Mix and incubate at 37 °C for 1 hour in a humidity chamber. If necessary, use Hydrophobic Coverslips.	
8	Immerse samples in 1X TdT Stop Buffer for 5 minutes at room temperature to stop labeling reaction.	
9	Wash samples 2 times in deionized water for 5 minutes each at room temperature.	This step removes unbound conjugate.
10	Cover sample with 50 µl of Strep-HRP solution and incubate for 10 minutes at 37 °C. If necessary, use hydrophobic coverslips.	Follow color development under the microscope to determine time of incubation.
11	Wash samples 2 times in 1X PBS for 2 minutes each.	
12	Immerse samples in DAB solution for 2 to 7 minutes.	Use caution when handling DAB solution.
13	Wash samples in several changes of deionized water for 2 minutes each.	
14	Proceed to Counterstaining and Preparation for Viewing.	

VI. Counterstaining and Preparation for Viewing

Cells and tissues may be counterstained with Methyl Green. Glass coverslips can be held in fine tipped forceps and dipped individually into the stains and ethanols. Spot only 25 µl mounting medium onto a clean glass slide and mount the coverslip, cell side down, onto the slide. If a plastic support was used for cell culture, do not pass through xylenes.

Method A (for most cells and tissues)

1. Immerse samples in deionized water for 2 minutes.
2. Immerse samples for 5 seconds to 5 minutes in Methyl Green.
3. Wash slides sequentially by dipping ten times each in:
    a. Deionized water
    b. 70% ethanol, 2 changes
    c. 95% ethanol, 2 changes
    d. 100% ethanol, 2 changes
    e. Xylenes, 2 changes
4. Wipe off excess xylenes from the back of the slide and lay slide flat.

5. Place one drop, about 50 µL, of mounting medium from a 100 µL pipet onto sample.
6. Lower glass coverslip onto sample and apply gentle even pressure to expel air bubbles.
7. Leave slides flat overnight to allow mounting medium to harden
8. Store slides in the dark.

APPENDIX H

Collagenase Tissue Digestion for Porcine Tendon

Collagenase solution (sterile filtered): 20 mg/ml Bovine Serum Albumin (Fraction V) in DMEM (1 g/L glucose) + 1% Am/AB + 2mg / ml collagenase type I (Worthington – MX1D12644: 249 U/mg)

Directions:

1. In an aseptic cell culture hood, rinse tendon tissue once in 20 ml of sterile 1x PBS to remove any excess blood.
2. Cut tendons into approximately 3 x 3 mm pieces/cubes with sterile scalpel blades in a sterile petri dish.
3. Weigh each cube of tendon separately and place individually in wells of a 24-well plate.
4. Add 2 mL of sterile filtered collagenase solution to each well containing a tendon sample and incubate at 37°C overnight (> 15 hours) at 86 RPM (VWR Incubating Orbital Shaker).
5. Stop collagenase by adding FBS (10% of volume used in step 5 so about 200 μL).

Source: Mazzocca, A. D., Chowaniec, D., McCarthy, M. B., Beitzel, K., Cote, M. P., McKinnon, W., & Arciero, R. (2012). In vitro changes in human tenocyte cultures obtained from proximal biceps tendon: Multiple passages result in changes in routine cell markers. *Knee Surgery, Sports Traumatology, Arthroscopy, 20*(9), 1666-72.

APPENDIX I

Dimethylmethylene Blue (DMMB) Assay Protocol

Materials and Reagents

1. Dimethylmethylene blue (DMMB) (Sigma-Aldrich, catalog number: 341088)
2. NaCl
3. Glycine (Sigma-Aldrich, catalog number: 410225)
4. Glacial Acetic acid (Sigma-Aldrich, catalog number: S7653)
5. Tris-Base (Merck KGaA, catalog number: 648310)
6. Bovine chondroitin 4-sulfate as standard (Sigma-Aldrich, catalog number: C9819)
7. DMMB reagent (see Recipes)

Equipment

1. Plate mixer (VWR International, catalog number: 89202-332)
2. Cover adhesive (R&D Systems, catalog number: DY992)
3. Microplate reader with 525 nm (BioTek Instruments, catalog number: 11-120-531)
4. 96 well microplate spectrophotometer with 525 nm filter set (Thermo Fisher Scientific, catalog number: 51119200)
5. Microplate shaker (VWR International, catalog number: 97043-608)

Procedure

1. Prepare DMMB reagent and paper filter using Whattman® 3MM. The pH of this solution is around 3.0. To prepare 1 L dye solution, dissolve 16 mg DMMB in 1 L water containing 3.04 g glycine, 1.6 g NaCl and 95 ml of 0.1 M Acetic Acid.
2. Prepare standard solution of chondroitin 4 sulfate (500 µg/ml in H2O). Prepare standard curve as stated in the table bellow.
3. Pipet the standard stock solution and complete the volume to 20 µl with H2O into the 96 well microplate.
4. Pipet 20 µl of each sample into the microplate.
5. Add 200 µl of DMMB to each sample and shake the plate of a plate shaker for 5 sec.
6. Read the absorbance using a plate reader at 525 nm immediately.

Std (µg/ml)	Vol (µl) of 500 µg/ml std	vol H_2O (µl)	vol DMMB (µl)
0	0	20	200
1.25	2.5	17.5	200
2.5	5	15	200
5	10	10	200
7.5	15	5	200
10	20	0	200

Notes

1. DMMB assay can normally be performed on samples with high detergent and salt concentrations; however the standard curve should be prepared in the same solution.
2. Avoid to performing the assay on samples in high albumin or serum concentrations, which may interfere with the assay (Warren, 2000).
3. Some groups have reported the interference of DNA in the DMMB assay; however, decreasing the pH to approximately 3 and increasing salt concentrations makes the interference of DNA negligible.
4. DMMB requires the length of glycosaminoglycan chain be over a tetrasaccharide.
5. DMMB reacts with the sulfate group of the GAG chain and therefore will not work with unsulfated GAGs such as hyaluronic acid.
6. Further information can be acquired by utilizing the carbazole reaction (sensitivity from 1 to 20 μg) to assay the carboxyl groups of the uronic acid for heparin sulfate, chondroitin sulfate and dermatan sulfate and/or anthrone reaction to assay the hexose group for keratan sulfate (Mort and Roughley, 2007).
7. The DMMB can also be very efficient when performing chromatography to rapidly assay for fractions containing GAGs (Burton-Wurster et al., 2003).
8. The DMMB-GAG complex that is formed results in the immediate formation of turbidity, however this complex starts to precipitate within 10 min, therefore the absorbance measurement should be performed immediately.

Recipes

1. DMMB reagent
   Dissolve 16 mg DMMB, 3.04 g glycine, 1.6 g NaCl and 95 ml of 0.1 M acetic acid and complete the volume to 1 L
   Filter (0.45 μm)
   Protect from light
   Do not use if precipitate is present in the solution

Source: http://www.bio-protocol.org/e1236

APPENDIX J
Schematic for Mechanical Testing

The following instructions are adapted from *Separation of Bovine Achilles Tendon Ends Repaired with Krackow and Modified Mason-Allen Suture Technique Under Cyclic Loading: A Biomechanical Study* (J.T. Kim et al.) and are for the mechanical testing of a tendon using a servohydraulic testing machine.

1. The distal end (osseous junction) of the specimen was cemented and fixed securely into a round plastic pot.
2. A nylon strap was then sewn to the proximal end (muscular junction) of the specimen using nylon suture.
3. The specimen was positioned into a servohydraulic testing machine (Instron Model #8874) base where the plastic pot was anchored to the lower testing frame platform
4. The nylon strap was then secured to the actuator of the test frame using a servohydraulic clamp. Dry ice was fixed to the nylon strap to freeze the proximal portion of the tendon and adhere it to the strap material.